The
ENGINEERS' DIGEST

REVIEW OF ENGINEERING PROGRESS ABROAD

VOL. V. No. 8 OCTOBER 1944

CHURCHILL CENTRELESS GRINDING MACHINES.
Built for precision work and continuous high production.

THE CHURCHILL MACHINE TOOL CO. LTD., BROADHEATH, Nr. MANCHESTER

THE ENGINEERS' DIGEST

REVIEW OF ENGINEERING PROGRESS ABROAD

Published Monthly at 120, Wigmore Street, London, W. 1.

Publishers : **ENGINEERS' DIGEST LTD.** – – – – Telephone : WELBECK 9357

Advertisement Dept. – 120, Wigmore Street, London, W.1 – Telephone : Welbeck 9357

Distribution – – E. & F. N. SPON, LTD., 57, Haymarket, London, S.W.1
Telephone : Whitehall 1860. Telegrams : Fenspon, Lesquare, London

Editorial Dept. – – 120, Wigmore Street, London, W.1. – Telephone : Welbeck 9357

Subscriptions to : ENGINEERS' DIGEST LTD., 120, Wigmore Street, London, W.1, or
E. & F. N. SPON, LTD., 57, Haymarket, London, S.W.1

ANNUAL SUBSCRIPTION OF 12 NUMBERS, £2 2s. SINGLE COPIES, 4s. 6d.

ADVISORY COMMITTEE

J. F. ALCOCK, B.A., A.M.I.Mech.E.
R. W. ALLOTT, M.A., A.R.Ae.S.
E. ALTON, D.Eng., A.M.Inst.B.E.
H. H. ASBRIDGE, M.B.E., M.I.Mech.E.
R. W. AYERS, M.I.W.
Col. J. BOWDEN, M.Inst.C.E., M.I.Mech.E.
H. H. BROUGHTON, M.I.Mech.E.
F. BUCKINGHAM, B.Sc., A.M.Inst.C.E., A.M.I.Mech.E.,
T. H. BURNHAM, B.Sc. (Lond.), A.M.I.Mech.E. [A.M.I.E.E.
I. S. CASWELL, M.Sc., M.I.Mech.E.
G. C. SAFFERY COOPER.
J. DICK, Ph.D., B.Sc., A.M.I.Mech.E.
D. FIFE, M.I.Mech.E.
G. E. FOXWELL, D.Sc. (Lond.), F.Inst.P., F.Inst.F., M.Inst.
R. GRIFFITHS, M.Sc. [Gas.E.
H. HEYWOOD, Ph.D., M.Sc. (Eng.), A.M.I.Mech.E.
O. HURST, M.Inst.N.A.
Capt. J. S. IRVING, M.I.Mech.E., M.I.A.E., A.F.R.Ae.S., M.S.A.E.
F. C. JOHANSEN, M.Sc. (Eng.), M.I.Mech.E., F.R.Ae.S., M.I.Loco.E.
W. J. KEARTON, D.Eng., M.I.Mech.E., A.M.Inst.N.A.
Prof. W. KERR, Ph.D., M.I.Mech.E.
G. V. LOMONOSOFF, Dr.Ing., M.I.Mech.E.
B. J. LYMER, M.I.Mech.E.
D. T. MacIVOR, M.I.Mech.E., M.Cons.E.
W. O. MANNING, F.R.Ae.S.
R. B. MATTHEWS, Wh.Ex., A.M.Inst.C.E., M.I.E.E., F.R.Ae.S
Prof. A. L. MELLANBY, D.Sc., LL.D., M.I.Mech.E.
J. H. R. RATCLIFFE, B.Sc. (Eng., Hons.), M.I.Mech.E.
Col. C. W. D. ROWE.
W. A. SCOBLE, D.Sc., A.R.C.Sc., M.I.Mech.E.
P. W. SEEWER, D.E. (Zurich), M.Inst.C.E., M.I.Mech.E.
Prof. S. PARKER SMITH, D.Sc., M.I.E.E., A.M.Inst.C.E.
C. E. H. VERITY, A.M.Inst.C.E., A.M.I.E.E., A.M.I.Mech.E.
E. G. WALKER, F.C.G.I., B.Sc. (Eng.), M.Inst.C.E., M.I.Mech.E., M.Am.Soc.C.E.
Major F. L. WATSON, M.Inst.C.E., M.I.Mech.E.
G. WATSON, M.Inst.C.E., M.I.Mech.E.
C. H. WOODFIELD, M.I.Mech.E., M.I.Struct.E.
T. WRIGHT, Ph.D., M.Sc.
M. L. YATES, Ph.D., M.Sc.Tech., M.A. (Com.), M.I.Mech.E.

The Steel for those Tough Machining Jobs
"SABEN TENCO"
10% COBALT HIGH SPEED STEEL
SANDERSON BROS & NEWBOULD LTD SHEFFIELD ENG

CONTENTS

page

Analyzing the Jet Propulsion Engine 249
"The Engineers' Digest," Vol. 5, No. 8, p. 249.

Clamping Devices for Jigs and Fixtures 246
"The Engineers' Digest," Vol. 5, No. 8, p. 246.

Co-ordination of Insulation in High-Tension Plants 238
"The Engineers' Digest," Vol. 5, No. 8, p. 238.

Fuel Contents Gauge for Aircraft 223
"The Engineers' Digest," Vol. 5, No. 8, p. 223.

High-Pressure Locomotive, Type 232-P, with Individual Axle Drive of the S.N.C.F. 242
"The Engineers' Digest," Vol. 5, No. 8, p. 242.

Induction Furnaces for Melting Metals and Alloys 235
"The Engineers' Digest," Vol. 5, No. 8, p. 235.

Internal Shoe Brakes 230
"The Engineers' Digest," Vol. 5, No. 8, p. 230.

Measurement on Plasma Diffusion in Mercury Arcs 237
"The Engineers' Digest," Vol. 5, No. 8, p. 237.

Nose Wheel or Tail Wheel Undercarriage ? 225
"The Engineers' Digest," Vol. 5, No. 8, p. 225.

Novel Bending Device for Light Metal Tubing 241
"The Engineers' Digest," Vol. 5, No. 8, p. 241.

Remarks on Jet-Propulsion of Aircraft 221
"The Engineers' Digest," Vol. 5, No. 8, p. 221.

Simple Interferometer for Surface-Quality Measurement 247
"The Engineers' Digest," Vol. 5, No. 8, p. 247.

Yield Point and Stress Distribution in Bars and Tubes due to Plastic Bending 227
"The Engineers' Digest," Vol. 5, No. 8, p. 227.

AC

WELDING INCREASES WELDING SPEEDS

Many manufacturers change to ACTARC Welding Transformers—because they get the following advantages :—

The **MONTA** current range 15—200 amps

1 High Quality Welds Assured.
Molten pool of metal easily controlled, weld uniformly strong, no trouble from Arc blow.

2 Electrode loss reduced.
A. C. welding facilitates use of larger electrodes and often reduces stub-ends by 20%.

3 Saves Power and Essential Materials.
Consumption less than for D. C. welder of same rating, because of the high efficiency of Actarc transformer. Weight of active parts minimised.

4 Maintenance.
Reduced to nil.

Actarc transformers comply in every respect with the instructions issued by the Directorate of Industrial Electrical Equipment.

ACTARC SUREARC REGD. TRADE MARK

ARC MANUFACTURING CO., LTD.
PROPRIETORS OF THE SURE-ARC ELECTRODE CO. LTD
ACTARC WORKS, GOLDHAWK ROAD, LONDON, W.12

TELEPHONE: SHE 1151 TELEGRAMS: ACTIVARC, PHONE, LONDON. CABLES: ACTIVARC, LONDON. 2184

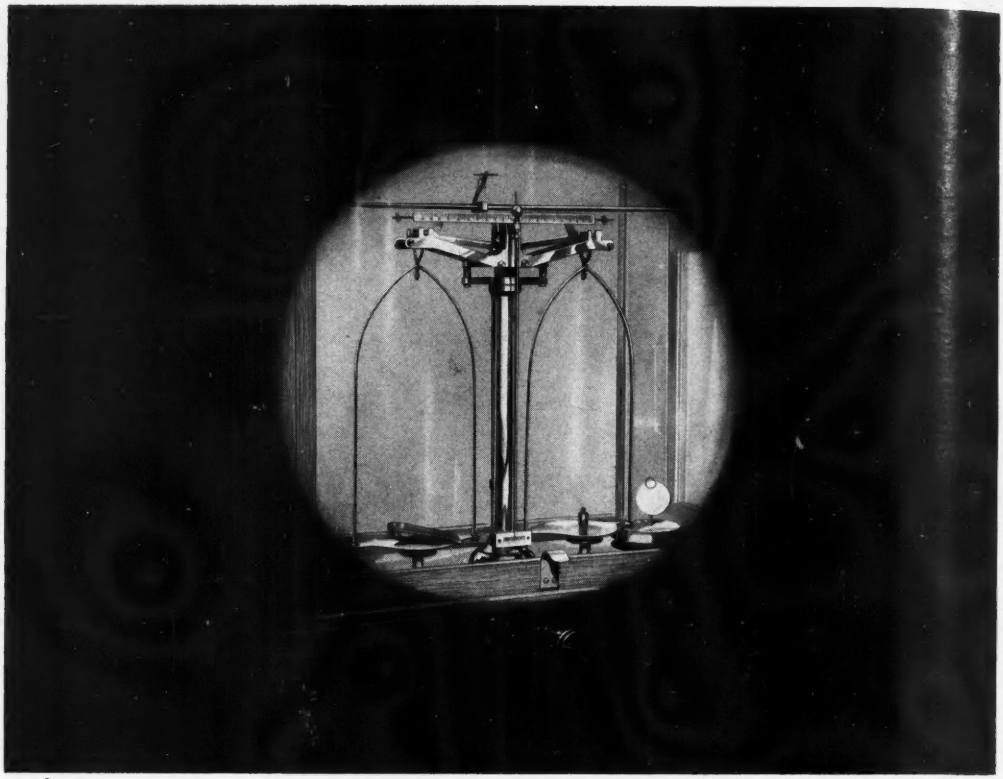

PRECISION

THE WICKMAN 10M.M. HIGH SPEED PRECISION AUTOMATIC — This machine was originally designed to cover a large variety of work for the wireless and electrical trades. In addition to producing parts for these two trades, it has now been adapted for more specialised work on which it has already proved highly successful. It is simple to tool for any component within its capacity and can be easily operated by female labour. Work up to 10mm. diameter by 4in. long can be accommodated and there are over 100 feeds for each spindle speed, covering all materials. May we send you full particulars?

Delivery is subject to Purchase and Priority Certificates issued by the M.T.C.

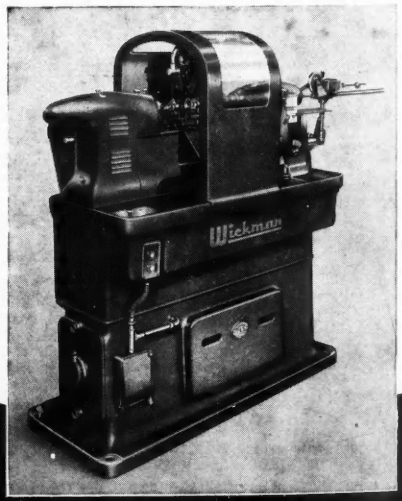

A.C. Wickman LIMITED

• COVENTRY • ENGLAND •

LONDON · BRISTOL · BIRMINGHAM · MANCHESTER · LEEDS · GLASGOW · NEWCASTLE

REMARKS ON JET-PROPULSION OF AIRCRAFT.

By Prof. Dr. J. Ackeret, Federal Technical College, Zurich. (From *Schweizerische Bauzeitung*, Vol. 12, No. 20 May 13th, 1944, pp. 235-237).

Independently of existing designs (Campini, Whittle), data on which are extremely scarce, it is attempted to present a picture of the possibilities as obtained by simple thermodynamic and mechanical considerations.

At first, it is noteworthy that the difference between the common propeller-engine propulsion and the jet propulsion is not quite as great as sometimes assumed.

Fig. 1 shows a propeller *Sch* driven by the engine *M*. The effect of the propeller (observed in a co-ordinate system moving with the aircraft) is to accelerate the influx airspeed W_e to the speed W_a. The "reaction" thus produced is equal to the thrust S of the propeller.

With Campini (Fig. 2), the propeller is placed in a duct, which thus acts as a blower G, and in addition the slipstream is heated by means of oil burners B. The efflux air, herewith, has not only increased speed W_e but also increased temperature. The blower creates pre-compression; by heating, volume increase at constant pressure is obtained, thus resulting in additional speed increase. The drawback of this method consists in the limitations imposed by the pre-compression in G and the temperature increase due to B, as with high values for these, W_a becomes too great. Although a great W_a gives great thrust, a high absolute speed $(W_a - W_e)$ of the airstream means a considerable loss of kinetic energy.

In the following arrangement (Fig. 3) which will be considered more closely, a variation is effected insofar as the blower is not driven by an aero-engine but by a gas turbine, having the burners B in front of the turbine inlet stream; thereby the design becomes more elegant, and probably the plant will also be lighter.

An insight into the working cycle can be obtained by reference to a schematic entropy-diagram (Fig. 4), which moreover affords the possibility of estimating the fuel consumption.

Let us consider the change of state of one kilogram of air when the air speed is W_1 and the altitude of flight corresponds to the absolute temperature T_1. In the duct entry the airspeed W_1 is decelerated to W_2. With a very small inaccuracy W_2 can be put equal to zero.

The temperature increase is: $$\frac{A W_1^2}{2 g c_p} = T_2 - T_1.$$

Substituting the speed of sound $a_1 = \sqrt{g k R T_1}$ and the Mach number $M_1 = \frac{W_1}{a_1}$,

we have $$\frac{T_2}{T_1} = 1 + \frac{k-1}{2} M_1^2 = \overline{M}$$

for air ($k = 1.4$), thus $$\overline{M} = 1 + 0.2\, M_1^2 \quad .. \quad (1)$$

The compression which follows can be expressed by the corresponding adiabatic temperature ratio

$$\vartheta = \frac{T_3}{T_2} \quad .. \quad .. \quad .. \quad (2)$$

It is for: $\frac{p_3}{p_2}$ =	1.5	2	2.5	3	4
ϑ =	1.123	1.219	1.299	1.369	1.487

For compression in the compressor the efficiency η_K is to be introduced, so that

$$T_4 - T_2 = \frac{T_3 - T_2}{\eta_K}; \quad \frac{T_4}{T_1} = \overline{M}\left(1 + \frac{\vartheta - 1}{\eta_K}\right) \quad (3)$$

Heating by burners from T_4 to T_5 takes place, which is expressed as

$$T_5 = K T_1 \quad .. \quad .. \quad .. \quad (4)$$

Should the expansion to atmospheric pressure be simply adiabatic, the temperature T_8 would be reached:

$$\frac{T_5}{T_8} = \frac{T_3}{T_1}$$

For adiabatic expansion between equal pressures,

$$\frac{T_8}{T_1} = \frac{T_5}{T_3} = \frac{KT}{\overline{M}\vartheta T_1} = \frac{K}{\overline{M}\vartheta} \quad .. \quad .. \quad (5)$$

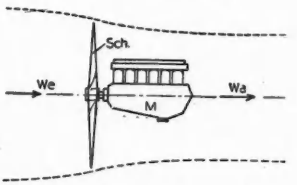

Fig. 1. **Normal propeller propulsion.**

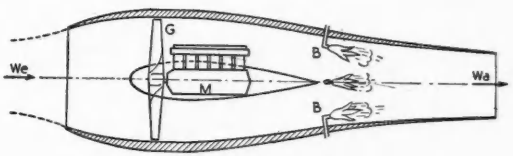

Fig. 2. **The Campini-system of jet propulsion.**

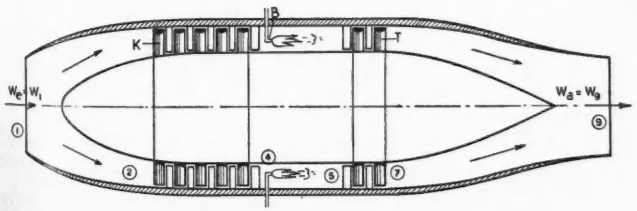

Fig. 3. **Jet propulsion with gas turbine.**
Heating occurs between compressor K and turbine T. Numerals in circles refer to co-ordinated points in the entropy diagram Fig. 4.

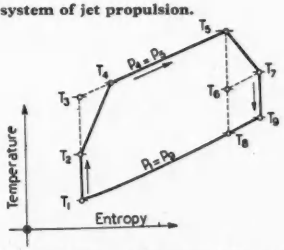

Fig. 4. **Entropy-diagram (schematic) of the cycle according to arrangement in Fig. 3.**

A part of the pressure drop will be consumed in the turbine, namely, just as much as to cover the work spent by the compressor. With the efficiency of the turbine η_T we have

$$\frac{T_3 - T_2}{\eta_K} = (T_5 - T_6)\,\eta_T$$

and $$T_4 - T_2 = T_5 - T_7$$

Herewith T_6 and T_7 are given:

$$\frac{T_6}{T_1} = K - \overline{M}\,\frac{\vartheta - 1}{\eta_K\,\eta_T} \qquad .. \quad (6)$$

$$\frac{T_7}{T_1} = K - \overline{M}\,\frac{\vartheta - 1}{\eta_K} \qquad .. \quad (7)$$

Finally, it follows, as the expansion between equal pressures

$$\frac{T_6}{T_8} = \frac{T_7}{T_9}$$

$$\frac{T_7 - T_9}{T_6 - T_8} = \frac{T_7}{T_6}$$

and thus, (eqs. 5, 6 and 7)

$$T_7 - T_9 = T_1\left(K - \overline{M}\,\frac{\vartheta - 1}{\eta_K\,\eta_T} - \frac{K}{\overline{M}\,\vartheta}\right)\frac{K - \overline{M}\,\dfrac{\vartheta - 1}{\eta_K}}{K - \overline{M}\,\dfrac{\vartheta - 1}{\eta_K\,\eta_T}} \qquad (8)$$

(*Continued in the next column.*)

The efflux speed W_9 can be found from

$$\frac{A\,W_9^2}{2g\,c_p} = T_7 - T_9$$

to be

$$W_9 = a_1\sqrt{\frac{2}{k-1}} \times \sqrt{K = \frac{\left(1 - \overline{M}\,\dfrac{\vartheta - 1}{\eta_K\,\eta_T K} - \dfrac{1}{\overline{M}\,\vartheta}\right)\left(1 - \overline{M}\,\dfrac{\vartheta - 1}{\eta_K K}\right)}{\left(1 - \overline{M}\,\dfrac{\vartheta - 1}{\eta_K\,\eta_T K}\right)}} \qquad (9)$$

Calorie: to be spent per kg.:

$$c_p\,(T_5 - T_4)$$

The thrust per kg./sec. according to the momentum theorem: $s = \dfrac{1}{g}\,(W_9 - W_1)$

Herefrom, the propulsive efficiency is

$$\eta = \frac{A\,s\,W_1}{c_p\,(T_5 - T_4)} = \frac{A}{g}\,\frac{W_1^2\left\{\dfrac{W_9}{W_1} - 1\right\}}{c_p\,(T_5 - T_4)} \qquad (10)$$

On substituting the values obtained above

$$\eta = \frac{2\,(\overline{M} - 1)}{K - \overline{M}\left(1 + \dfrac{\vartheta - 1}{\eta_K}\right)} \cdot \left\{\sqrt{K\,\frac{\left(1 - \overline{M}\,\dfrac{\vartheta - 1}{\eta_K\,\eta_T K} - \dfrac{1}{\overline{M}\,\vartheta}\right)\left(1 - \overline{M}\,\dfrac{\vartheta - 1}{\eta_K K}\right)}{(\overline{M} - 1)\left(1 - \overline{M}\,\dfrac{\vartheta - 1}{\eta_K\,\eta_T K}\right)}} - 1\right\} \qquad (11)$$

The *total thrust* S can be calculated when the jet area F_9 is known.

We have: $S = \dfrac{1}{g}\,F_9\,W_9\,\gamma_9\,(W_9 - W_1)$; further: $\gamma_9 = \dfrac{p_9}{RT_9} = \dfrac{p_1}{RT_9}$ and $T_9 = \dfrac{T_8}{T_6}\,T_7$

$$S = F_9\,a_1\sqrt{\frac{2}{k-1}}\,\rho_1\,\overline{M}\,\vartheta\left\{\sqrt{\frac{1}{K}\,\frac{\left(1 - \overline{M}\,\dfrac{\vartheta - 1}{\eta_K\,\eta_T K} - \dfrac{1}{\overline{M}\,\vartheta}\right)\left(1 - \overline{M}\,\dfrac{\vartheta - 1}{\eta_K\,\eta_T K}\right)}{\left(1 - \overline{M}\,\dfrac{\vartheta - 1}{\eta_K K}\right)}}\right\} - \left\{a_1\sqrt{\frac{2}{k-1}}\right.$$

$$\left.\sqrt{K\,\frac{\left(1 - \overline{M}\,\dfrac{\vartheta - 1}{\eta_K\,\eta_T K} - \dfrac{1}{\overline{M}\,\vartheta}\right)\left(1 - \overline{M}\,\dfrac{\vartheta - 1}{\eta_K K}\right)}{\left(1 - \overline{M}\,\dfrac{\vartheta - 1}{\eta_K\,\eta_T K}\right)}} - W_1\right\} \qquad (12)$$

In the case of take-off, for the *static thrust* ($W_1 = 0$), $\overline{M} = 1$

$$S = S_0 = F_9\,a_1^2\,\frac{2}{k-1}\,\rho_1\,\vartheta\left(1 - \frac{\vartheta - 1}{\eta_K\,\eta_T K} - \frac{1}{\vartheta}\right) \qquad (13)$$

The discussion of eq. (11) gives the following result: With efficiencies that can be realized, $\eta_K = 0.8$ and $\eta_T = 0.85$, the propulsive efficiency as a function of maximum temperature has been plotted (Fig. 5); herein $\vartheta = 1{,}30$ and $\overline{M} = 1{,}10$ are assumed.

This corresponds to a speed of 800 km./hr. in 6000 m. altitude ($T_1 = 250$ deg.), and a compression ratio of 2.5 in the compressor, requiring a rather high number of stages. The maximum efficiency in Fig. 5, 14.3 per cent, is very low. A very poor engine (fuel consumption 280 gr. h.p./hr.) and inefficient propeller ($\eta_P = 0.635$) would give an equally low overall efficiency. As Fig. 6 shows, a higher temperature ratio ϑ would give better efficiency; however, this would necessitate very high compression ratios (4.0) for improvements that would fall into the scales.

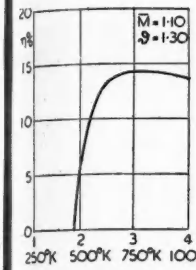

Fig. 5. **Efficiency as a function of maximum temperature.**

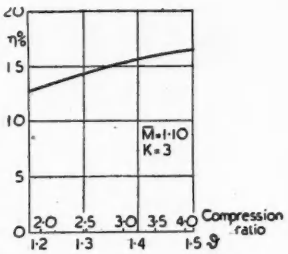

Fig. 6. **Efficiency of the jet propulsion system shown in Fig. 3 as a function of the compression and temperature ratios in the compressor.**

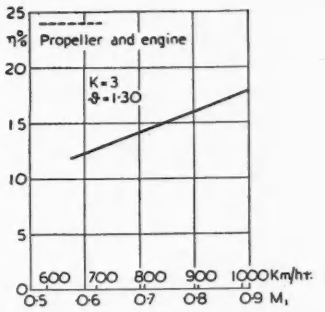

Fig. 7. **Efficiency as a function of air-speed and Mach number.**

Dotted line : propulsive efficiency of propeller and engine calculated for fuel consumption of modern types.

The pure jet propulsion has, at *very high* speeds, an efficiency comparable to that obtained by present-day orthodox propulsion. Fig. 7 shows that this speed is of the order of 1000 km./hr. But even at lower speeds, say $\eta_{total} = 13$ per cent, corresponding to 700 km./hr., a fuel *excess weight* is spent in but two hours which is identical to the weight of a good aero-engine of equivalent power. Thus, it is clear that an arrangement such as in Fig. 3 is possible for flights of extremely *short duration* only.

The opinion is often voiced that the propeller is not suitable for high speeds (700 to 900 km./hr.). To this, it should be said that propellers can be designed so that their tip speeds are far below the speed of sound. Of course, a higher degree of reduction and greater diameters will be required. The efficiencies remain still good (counter rotating propellers offer here many new possibilities).

An increase in speed beyond 900 km./hr. requires immense power. Today small fighters powered with 1000 h.p. reach a speed of 550 km./hr. Should the speed be increased to 900 km./hr. at the same altitude, at least 4000 h.p. would be required, presupposed that this power could be accommodated within the same space. Obviously, the available fuel is sufficient for flights of short duration only. In principle, greater efficiency could be achieved if one could succeed in using a *heat exchanger* by which the heat of the efflux stream could be recovered, and added to the heat at the turbine inlet. It is, however, questionable whether the weights and volumes required herefor could be kept in economic limits.

Summing up, it can be said that pure jet propulsion using a turbine according to Fig. 3, is, from the point of view of fuel consumption, uneconomical below speeds of 900 km./hr., as compared with present-day propeller propulsion. Its use would be justifiable if the design weight could be reduced, or where higher speeds, even for short duration, are required (fighter aircraft).

FUEL CONTENTS GAUGE FOR AIRCRAFT.

By E. CZERLINSKY and J. ZEYNS. (From *Luftfahrtforschung*, Vol. 20, Nos. 8/9, October 16th, 1943, pp. 263-267)

Report of the German Institute of Aeronautical Research, DVL, Berlin—Adlershof.

Of the many possible principles of measuring in flight the variable contents of fuel tanks, preference is given to weighing, which can be done in the accelerated state, by comparison with a constant mass. The principle of the present method is seen by reference to Fig. 1. Both the fuel tank and the comparative weight are suspended from springs not far from each other. The spring constants are chosen so as to make the spring extensions (a) and (b) of the same order. Both extensions are proportional to the same accelerations and to the cosine of identical inclinations (position). Thus, the ratio a/b is independent of position and acceleration, and a measure for the mass of the tank (including fuel) relative to the given comparative mass. The accuracy of indication is ± 3 per cent of the maximum fuel contents at accelerations for up to 2g. and for positional changes of 30 deg. from the horizontal. The extensions (a) and (b) are translated into electrical quantities by the fact that the electric resistance of wire changes when strained within the elastic limit. The resistance wire used is of constantan, of 0.06 mm. dia. Linear increase of resistance ΔW (i.e., within the range of validity of Hook's law) extends up to 40 kg./mm². at a

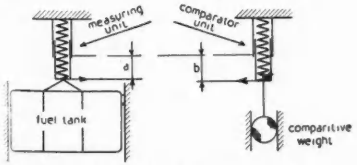

Fig. 1. **Principle of Measurement.**

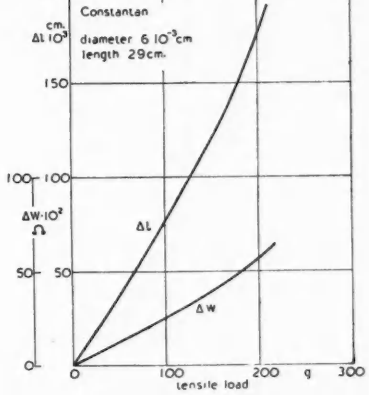

Fig. 2. **Properties of constantan due to tension.**

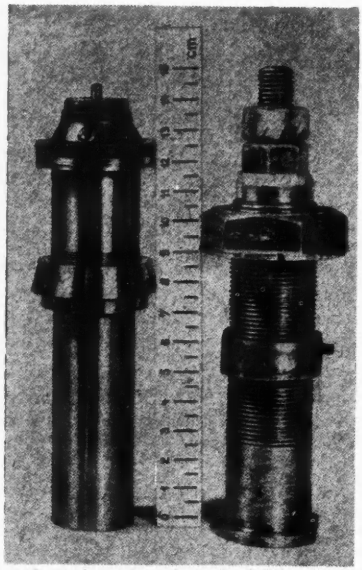

Fig. 3. **Measuring unit and standard tightening screw.**

tensile strength of 80 kg./mm². This property and the elongation Δl are plotted in Fig. 2 against the tensile load.

The external form of the measuring unit in which the constantan wires are employed has been adopted to the need of replacing standard tightening screws of metal belts which carry the tank. Both the measuring unit and the old standard tightening screw are shown in Fig. 3 for comparison. The construction of the measuring unit is shown in Fig. 4. It can be seen that the tightening screws of the usual metal belts are now housed in the tubular part *B* of the measuring unit. *B* is guided in the tubular member *R*, which is fixed by means of a conical nut to the structure frame. The tank weight is transmitted by *B* to the structure frame through member *G*, which represents the spring. The extension of the spring *G* is about 0.05 mm. for a 100 kg. tank load, and is transferred to constantan measuring wires which are mounted between two amber bushes so as to relieve them when load is applied to member *G*. The advantage of this arrangement is that the wires do not fail under excess loads, and the initial tension can be of the magnitude of the elastic limit of the wire when the tank is empty. (The initial tension of the measuring wires is set by means of screw *S*, and simultaneously the electric resistance of the wires is measured). By this means the quantity to be measured, i.e., the ratio of change in electric resistance to change in load, reaches its optimum value.

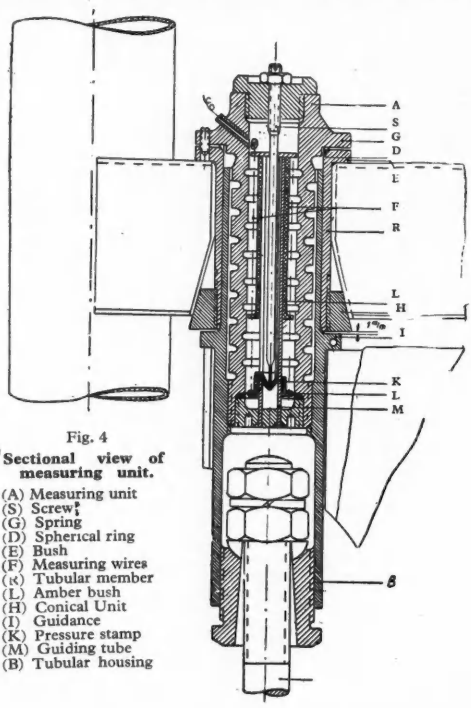

Fig. 4

Sectional view of measuring unit.

(A) Measuring unit
(S) Screw
(G) Spring
(D) Spherical ring
(E) Bush
(F) Measuring wires
(R) Tubular member
(L) Amber bush
(H) Conical Unit
(I) Guidance
(K) Pressure stamp
(M) Guiding tube
(B) Tubular housing

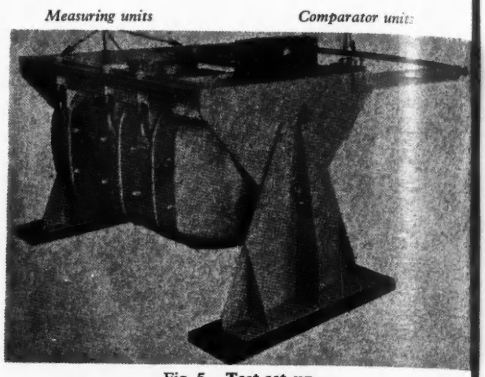

Fig. 5. **Test set-up.**

At an initial resistance of 36Ω this is about $60 \times 10^{-3}\Omega$ per 100 kg. of load.

The effect of temperature changes is eliminated by invar-parts in screw *S*, and other precautions taken such as doubling the measuring wires, or suitable oil filled into part *G*, and the use of constantan assembled by welding to prevent thermo-currents, has enabled accuracy to be maintained over a period of years. Fig. 5 shows the test set-up, the frame of which can be tilted. The tank is carried by six measuring units, and there are two comparator units. In the black case the amplifier and indicator are housed.

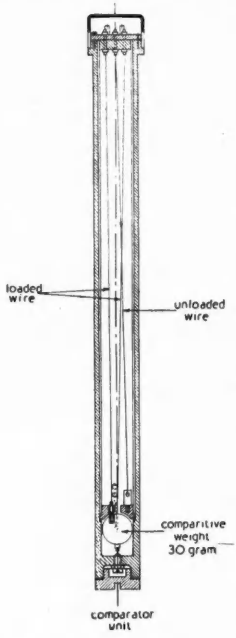

Fig. 6. **Comparator unit.**

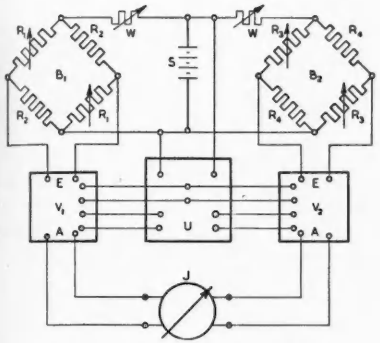

Fig. 7. **Wiring diagram of contents gauge.**

The measuring units are simpler than the comparator units which are necessary to obtain immunity from acceleration and positional changes. As Fig. 6 shows, the comparator unit contains a ball of about 30 gram weight, suspended from a constantan wire and guided laterally, and an equally long but unloaded wire compensates for temperature effects. The ratio of the maximum fuel mass to the comparative mass is 15000:1.

The wiring diagram of the contents gage is shown in Fig. 7. The wires of the measuring unit are shown as resistances R_1, the doubling wires which are unstrained are the resistances R_2 forming with R_1 a bridge B_1. Bridge B_2 is formed by the two comparator units containing the loaded wires R_3 and the unloaded wires R_4. Both bridges are supplied by accumulator S. The voltage at the brackets E is regulated by the resistances W and a transformer U is joined to S, giving

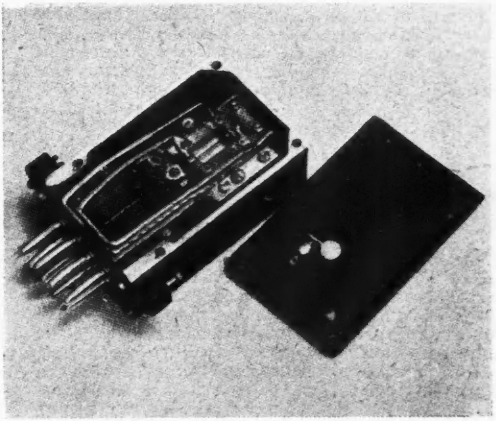

Fig. 8. **Bolometer amplifier.**

the relay-voltage. The indicator I measures the ratio of the currents given by the two bolometer amplifiers V_1 and V_2. The total energy requirement is about 15 watts. The bolometer amplifier has been made by Siemens, and is shown in Fig. 8.

Flight tests made with the installation extended over a period of three months, during which time no deterioration of the accuracy of indication was observed. Accurate readings were obtained at accelerations up to 3 g. and positional changes of about 50 degrees. Only under sideslip of the aircraft were errors noted, and these were due to oscillations in the coil systems of the bolometer amplifiers.

NOSE WHEEL OR TAIL WHEEL UNDERCARRIAGE

By P. JARAY, SOLOTHURN. (From *Flugwehr und Technik*, Vol. 6, No. 3, March, 1944, pp. 80-84).

THE greatest drawback with the tail wheel undercarriage is the necessity of keeping the angle of incidence of the wing during landing within narrow limits. These limits are the angle of stall and that safe angle which prevents a nosing over of the aircraft. The minimum landing speed is given approximately by

$$V_{min} = 4\sqrt{p/C_{L\,max}} \quad .. \quad .. \quad (1)$$

where P is the specific wing loading (kg./m.²) and $C_{L\,max}$ the maximum lift coefficient. The angle of incidence at this lift coefficient corresponds to the three-point landing. It is this type of landing that makes the tail-wheel undercarriage difficult to land with even for experienced pilots. Lift increasing devices make little difference to this fact. With an increased lift coefficient however, it is possible to reduce the angle of incidence, i.e., to land with main wheels alone. To do this requires even greater skill because of the danger of nosing over or the tendency of jumping. The limitation on braking is a further drawback of the orthodox undercarriage, as with regard to the take-off the ratio x_A/h, i.e., the longitudinal distance between centre of gravity of aircraft and main wheel axis, and height of the centre of gravity above ground, cannot be greater than

$$x_A/h = 0.5 \ldots . 0.6 \quad .. \quad .. \quad (2)$$

Thus, the maximum available coefficient of friction dependent on surface conditions of the airfield

$$\mu = 0.6 \ldots . 1.0 \quad .. \quad .. \quad (3)$$

cannot be fully realized.

With the nose-wheel undercarriage there is no limitation as to the angle of incidence during landing. Any angle of incidence in wide limits around $C_{L\,max}$ is feasible. Braking can be fully applied at the instance of touch-down, fully utilizing the available coefficient of ground friction.

The two undercarriages can be best compared on hand of the moments due to a landing with cross-wind when the drifting aircraft is under an angle of yaw β to the direction of movement (Figs. 1 and 2). The external moment Ms is counteracted by moments due to ground friction alone. Aerodynamic forces being already small, can be neglected. With the notation of Fig. 1 for the tail-wheel undercarriage one can write

$$M_s < \mu_A Q_{A2}\left(\frac{s}{2}\cos\beta - x_A \sin\beta\right) - \mu_A Q_{A1}\left(\frac{s}{2}\cos\beta + x_A \sin\beta\right) + \mu_H Q_H \cdot x_H \sin\beta \quad .. \quad (4)$$

The braking forces μQ are given by

$$\mu_A Q_{A2} = \mu_A\left[G\frac{x_H}{2e} + P\left(\frac{h}{2e}\cos\beta + \frac{h}{s}\sin\beta\right)\right] \quad (5)$$

$$\mu_A Q_{A1} = \mu_A\left[G\frac{x_H}{2e} + P\left(\frac{h}{2e}\cos\beta - \frac{h}{s}\sin\beta\right)\right] \quad (6)$$

$$\mu_H Q_H = \mu_H\left(G\frac{x_A}{e} - P\frac{h}{e}\cos\beta\right) \quad .. \quad .. \quad (7)$$

With $P = E\mu Q$, we have

$$P = G\frac{x_A \mu_H + x_H \mu_A}{e + h\cos\beta\,(\mu_H - \mu_A)} \quad .. \quad .. \quad (8)$$

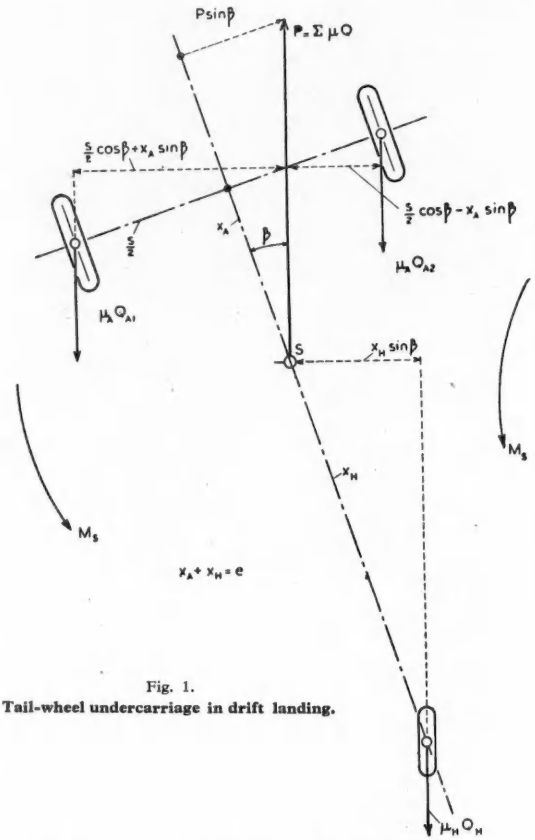

Fig. 1.
Tail-wheel undercarriage in drift landing.

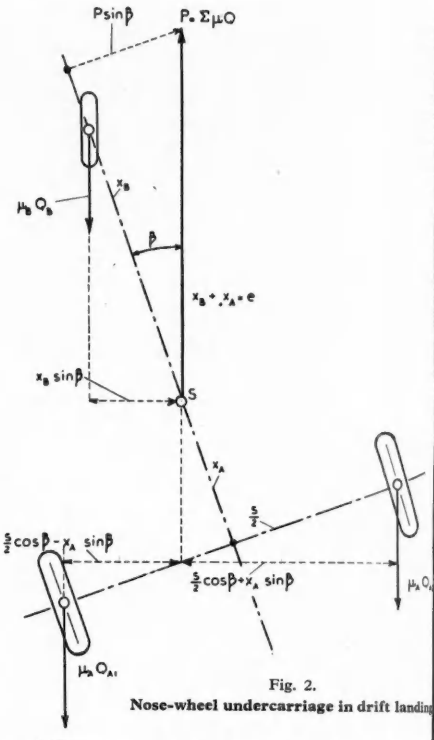

Fig. 2.
Nose-wheel undercarriage in drift landing

and after some transformations, and replacing cos β by 1 and sin β by β,

$$M_s < G\beta \frac{x_H(x_A - h\mu_A)}{\frac{e}{\mu_H - \mu_A} + h} \quad .. \quad .. \quad (9)$$

Similarly, for the nose-wheel undercarriage we obtain the following equations :

$$M_s < \left[\mu_A Q_{A2}\left(\frac{s}{2}\cos\beta + x_A \sin\beta\right) - \mu_A Q_{A1}\left(\frac{s}{2}\cos\beta - x_A \sin\beta\right) - \mu_B Q_B \cdot x_B \sin\beta\right] \quad (10)$$

$$\mu_A Q_{A2} = \mu_A\left[G\frac{x_B}{2e} - P\left(\frac{h}{2e}\cos\beta - \frac{h}{s}\sin\beta\right)\right] \quad (11)$$

$$\mu_A Q_{A1} = \mu_A\left[G\frac{x_B}{2e} - P\left(\frac{h}{2e}\cos\beta + \frac{h}{s}\sin\beta\right)\right] \quad (12)$$

$$\mu_B Q_B = \mu_B\left(G\frac{x_A}{e} + P\frac{h}{e}\cos\beta\right) \quad .. \quad .. \quad (13)$$

$$P = G\frac{x_A\mu_B + x_B\mu_A}{e + h\cos\beta(\mu_A - \mu_B)} \quad .. \quad (14)$$

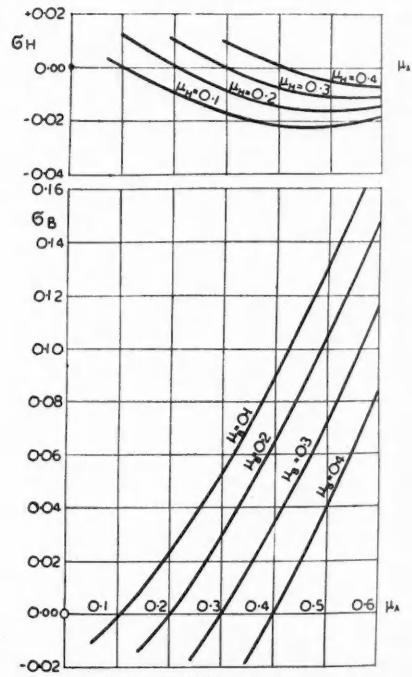

Fig. 3. **Stability diagram.**

$$M_s < G\beta \frac{x_B (x_A + h\,\mu_A)}{\frac{e}{\mu_A - \mu_B} + h} \quad .. \quad .. \quad (15)$$

Substituting in eqs. (g) the following practical values for the tail-wheel undercarriage

$$h = 0.25e, \quad x_A = 0.15e, \quad x_H = 0.85e \; .. \quad (16)$$

and in eq. (15) for the nose-wheel undercarriage

$$h = 0.62e, \quad x_A = 0.20e, \quad x_B = 0.80e \; .. \quad (17)$$

we obtain the stability parameters

$$\frac{M_s}{Ge_H\beta} < \sigma_H = \frac{a_H - b_H\mu_A}{\frac{1}{\mu_H - \mu_A} + c_H} \; .. \quad .. \quad (18)$$

and

$$\frac{M_s}{Ge_B\beta} < \sigma_B = \frac{a_B + b_B\mu_A}{\frac{1}{\mu_A - \mu_B} + c_B} \; .. \quad .. \quad (19)$$

which are plotted in Fig. 3 against μ_A for various values of μ_B and μ_H. It can be seen from the diagram that the nose-wheel undercarriage is stable, while the tail-wheel undercarriage is unstable.

For the ratio x_A/e the optimum value has been found to be between 0.2 and 0.25

Turning on ground requires a small x_A/e (or a large x_B/e).

The speed of turn should be $v < 2.1 \sqrt{\frac{s\,x_B}{h \tan \beta}}$ (20)

which shows that stability in turn is dependent on the width of track and the height of C.G above ground.

The article contains a table giving data of 33 nose-wheel types in the period 1936-1943. These have been mostly made public before and are omitted here. So are the detailed conclusions with regard to the advantages of the nose-wheel undercarriage. The author states, in summing up, that the favourable characteristics of the nose-wheel undercarriage are destined to play an important rôle in the further development of aircraft.

YIELD POINT AND STRESS DISTRIBUTION IN BARS AND TUBES DUE TO PLASTIC BENDING.

By ERIC BERNHULT. (From *Jernkontorets Annaler*, Vol. 127, No. 10, Oct., 1943, pp. 491-533).

THE question of the yield point due to bending has long been under scrutiny. Many experiments undertaken to clear this problem have shown that under bending a higher yield point is found as compared to that obtained from the tensile test. But the question as to whether this increase in yield point is apparent or actual has not yet been settled, not even by means of X-ray investigations. Recent investigations of the problem indicate, however, that bending stress does not increase the yield point but, that the numerical value of the yield point is the same both for tensile and for bending stresses. Under bending stress an apparent increase in yield point occurs, which is due to the shape of the sectional area, that is to say, the greater the concentration of material around the neutral axis, the higher is the apparent yield point.

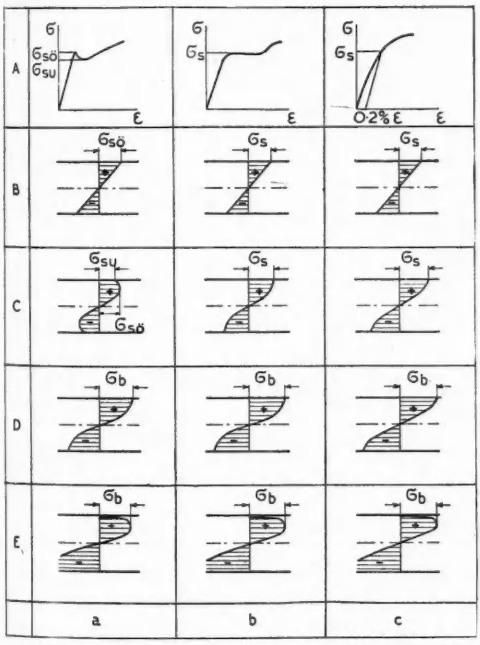

Figs. 1a, 1b, 1c. **Stress characteristics with bending of material with pronounced upper and lower yield points (a), without upper yield point (b), and without noticeable yield point (c).**

Considering a bent beam to be composed of an infinite number of fibres, each of which acts as a bar under tension or under compression, the author comes to the conclusion that no actual increase in the yield point takes place in bending, the stress conditions being determined by the tensile strength properties of the material. The appearance of the stress distribution characteristic through the cross section will depend upon whether the material has a pronounced lower and upper yield point, or no marked yield point at all.

The author contends that the bending moment—deflection curves are approximately straight lines up to the point where the elastic and the plastic bending moments are identical. But a noticeable deviation from the straight line takes place when the plastic moment begins to increase above the elastic moment. This point is designated by the author as the limit of bending proportionality, or *bp*-limit, and the apparent stress of the extreme fibre under tensile stress is denoted by σ'_p. Actually this stress may be either σ_{su} or σ_s—as indicated in Fig. 1a, 1b—or in certain cases it may equal $\sigma_{sö}$; while in a material without proper yield point, the extreme fibre stress will be higher as a rule than σ_s (0.2 per cent limit) as indicated in Fig. 1c.

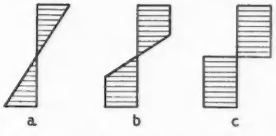

Fig. 2. **Elastic-plastic stress distribution.**

For the mathematical computation of the value of σ'_p, the stress distribution curve is replaced by straight lines, as shown in Fig. 2. With regard to the stress distribution indicated in Fig. 1b, this approximation is of little importance. The error resulting in cases Figs. 1a and 1c can be compensated for by an appro-

priate adjustment of the σ_s value. For all practical purposes this inaccuracy remains unimportant, in view of the experimental error involved in the measurement of yield point. The values of σ_s and σ_{-s} are, therefore, assumed to be constant to a certain depth of the sample shewn in Fig. 3 by the distance a from the neutral axis. In the case of a tube with an inner diameter d_i and an outer diameter d_y, it may either be $a < \frac{di}{2}$ or $a > \frac{di}{2}$

In the following r and R are substituted for $\frac{d_i}{2}$, and $\frac{d_y}{2}$ respectively.

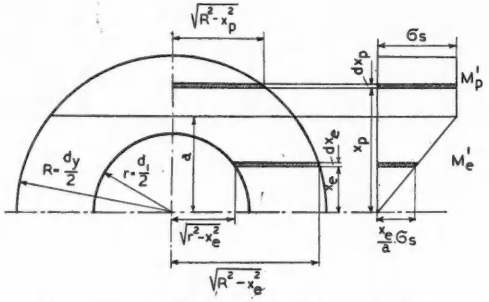

Fig. 3. **" bp-limit " diagram for thick-walled tube.**

Case I. Considering first the case of a thick-walled tube, outlined in Fig. 3, in which $a > r$, the plastic bending moment M'_p and the elastic bending moment M'_e are given by

$$M'_p = 4\sigma_s \int_a^R \sqrt{R^2 - x_p^2}\,.\,x_p\,dx_p$$

$$M'_e = 4\frac{\sigma s}{a}\left\{\int_o^r \sqrt{(R^2-x_e^2)}\,x_e^2\,dx_e - \int_o^r \sqrt{(r^2-x_e^2)}\,x_e^2\,dx_e + \int_r^a \sqrt{(R^2-x_e^2)}\,x_e^2\,.\,dx_e\right\}$$

By integration,

$$M'_p = \frac{4\sigma_s}{3}(R^2-a^2)\sqrt{R^2-a^2}$$

$$M'_e = \frac{4\sigma_s}{a}\left\{\frac{a}{4}\sqrt{R^2-a^2}\left(a^2-\frac{R^2}{2}\right)+\frac{R^4}{8}\sin^{-1}\frac{a}{R}-\frac{\pi r^4}{16}\right\}$$

As an approximation,

$$\sqrt{R^2-a^2} = R - \frac{a^2}{2R} - \frac{a^4}{8R^3}$$

and

$$\sin^{-1}\frac{a}{R} = \frac{a}{R} + \frac{a_3}{6R_3} + \frac{3a^5}{40\,R^5}$$

so that

$$M'_p = \frac{4\sigma s}{3}\left(R^3 - \frac{3a^2R}{2} + \frac{3a^4}{8R} + \frac{a^6}{8R_3}\right)$$

and $M'_e = \frac{4\sigma s}{a}\left(\frac{a^3R}{3} - \frac{a^5}{10R} - \frac{a^7}{32R^3} - \frac{\pi r^4}{16}\right)$

With $M'_p = M'_e$:

$$\frac{R_3}{3} - \frac{5a^2R}{6} + \frac{9a^4}{40R} + \frac{7a^6}{96R^3} + \frac{\pi r^4}{16a} = 0, \text{ and}$$

dividing by R^3 and making $\frac{a}{R} = \xi$, and $\frac{r}{R} = \eta$, it is

$$\frac{1}{3} - \frac{5\xi^2}{6} + \frac{9\xi^4}{40} + \frac{7\xi^6}{96} + \frac{\pi\,.\,\eta^4}{16\xi} = 0.$$ This can also be written thus :

$$35\,\xi^7 + 108\,\xi^5 - 400\,\xi^3 + 160\,\xi + 30\,\pi\,.\,\eta^4 = 0 \;..\; (1)$$

Case II. For $a < r$, characterising a thin walled tube, and denoting the plastic bending moment for the entire section by M''_p and the elastic moment by M''_e, it follows that from Fig. 4 that

$$M''_p = 4\sigma_s\left\{\int_a^r \sqrt{R^2-x_p^2} - \sqrt{(r^2-x_p^2)}\,x_p\,dx_p + \int_r^R \sqrt{R^2-x_p^2}\,x_p\,.\,dx_p\right\}$$

$$M''_e = \frac{4\sigma_s}{a}\int_o^a \left(\sqrt{R^2-x_e^2} - \sqrt{(r^2-x_e^2)}\right)x_e^2\,dx_e$$

Integration gives :

$$M''_p = \frac{4\sigma_s}{3}\left\{(R^2-a^2)\sqrt{(R^2-a^2)} - (r^2-a^2)\sqrt{(r^2-a^2)}\right\}$$

$$M''_e = \frac{4\sigma_s}{a}\left\{\frac{a}{4}\sqrt{(R^2-a^2)}\left(a^2-\frac{R^2}{2}\right) - \frac{a}{4}\sqrt{r^2-a^2}\left(a^2-\frac{r^2}{2}\right) + \frac{R^4}{8}\sin^{-1}\frac{a}{R} - \frac{r^4}{8}\sin^{-1}\frac{a}{r}\right\}$$

Substituting as before,

$$M''_p = \frac{4\sigma_s}{3}\left\{R^3 - \frac{3a^2R}{2} + \frac{3a^4}{8R} + \frac{a^6}{8R^3} - r^3 + \frac{3a^2r}{2} - \frac{3a^4}{8r} - \frac{a^6}{8r^3}\right)$$

$$M''_e = 4\sigma_s a^2\left(\frac{R}{3} - \frac{a^2}{10R} - \frac{a^4}{32R^3} - \frac{r}{3} + \frac{a^2}{10r} + \frac{a^4}{32r^3}\right)$$

With $M''_p = M''_e$, and dividing by R^3 and substituting $\frac{a}{R} = \xi$, and $\frac{r}{R} = \eta$, we get :

$$1 - \frac{5}{2}\xi^2 + \frac{27}{40}\xi^4 + \frac{7}{32}\xi^6 - \eta^3 + \frac{5}{2}\xi^2\eta - \frac{27\xi^4}{40\eta} - \frac{7\xi^6}{32\eta^3} = 0$$

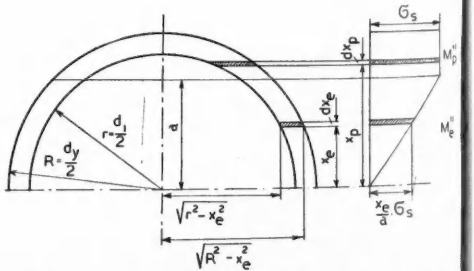

Fig. 4. **" bp-limit " diagram for thin-walled tube.**

which can also be written :

$$35\,\xi^8(\eta^2+\eta+1)+108\,\xi^4\eta^2+400\,\xi^2\eta^3-160\,\eta^3(\eta^2+\eta+1)=0 \quad .. \quad .. \quad (2)$$

It can be seen that the curves representing equations (1) and (2) intersect for $\xi = 0.85$ and $\eta = 0.85$. For $\eta = 0$, it is $\xi = 0.686$ and for $\eta = 1$, $\xi = 0.92$. Numerical values for the variation of ξ with η are given in Table I, the resulting curve is shown in Fig. 5.

From Table I and Fig. 5 it can be seen that equation (1) is valid for bars and for thick walled tubes up to $d_1/d_y = 0.85$, while equation (2) is applicable to thin-walled tubes with d_1/d_y ranging from 0.85 — 1.0. When the bp-limit is reached, the compression stress σ_s extends down to a distance " a " from the neutral fibre. In this case, the bending moment can be computed as follows :

Case I. $0 < d_1/d_y < 0.85$ (thick walled tube).

The basic equation $M_I = M'_p + M'_e = 2\,M'_p = 2\,M'_e$ can be written thus :

$$M_I = 4\sigma_s\left(\frac{R^3}{3}-\frac{a^2R}{6}+\frac{a^4}{40\,R}+\frac{a^6}{96\,R^3}-\frac{\pi\,r^4}{16\,a}\right), \text{ or}$$

$$M_I = \sigma_s\left(\frac{d_y^3}{6}-\frac{a^2d_y}{3}+\frac{a^4}{5\,d_y}+\frac{a^6}{3\,d^3{}_y}-\frac{\pi\,d_1^4}{64\,a}\right) \quad (3)$$

Furthermore, for an extreme fibre stress σ_s of a bent tube,

$$M_{bs} = W_b \,.\, \sigma_s = \frac{\pi}{32}\,.\,\frac{(d_y^4-d_1^4)}{d_y}\,.\,\sigma_s, \text{ and therefore}$$

$$\frac{M_I}{M_{bs}} = \frac{32}{\pi\left(1-\frac{d_1^4}{d_y^4}\right)}\left(\frac{1}{6}-\frac{a^2}{3\,d_y^2}+\frac{a^4}{5\,d_y^4}+\frac{a^6}{3\,d_y^6}-\frac{\pi\,d_1^4}{64\,a\,d_y^3}\right) \quad (4)$$

Similarly, in case II with $0.85 < d_1/d_y < 1$, referring to thin walled tubes

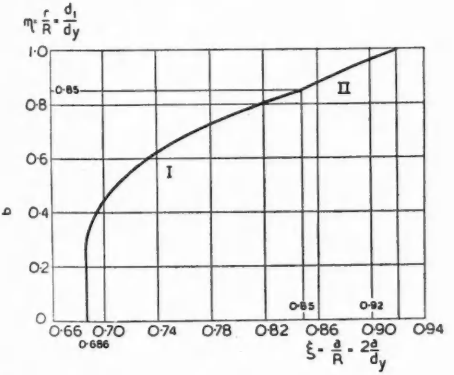

Fig. 5. ξ against η plotted for thick and thin-walled tubes.

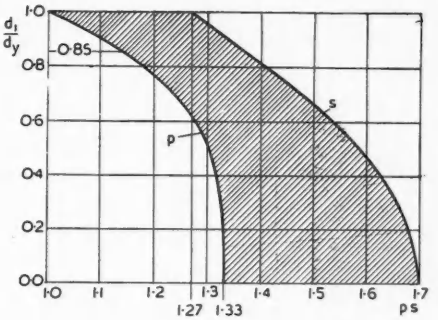

Fig. 6. p and s plotted against di/dy for thick and thin-walled tubes.

$$M_{II} = M''_p + M''_e = 2\,M''_p - 2M''_{e_2} \text{ and therefore :}$$

$$M_{II} = 4\,\sigma_s\left(\frac{R_3}{3}-\frac{a^2R}{6}+\frac{a^4}{40\,R}+\frac{a^6}{96\,R^3}-\frac{r^3}{3}+\frac{a^2r}{6}-\frac{a^4}{40r}-\frac{a^6}{96r^3}\right)$$

or :

$$M_{II} = \sigma_s\left(\frac{d_y^3}{6}-\frac{a^2d_y}{3}+\frac{a^4}{5\,d_y}+\frac{a^6}{3\,d_y^3}-\frac{d_1^2}{6}+\frac{a^2d_1}{3}-\frac{a^4}{5\,d_1}-\frac{a^6}{3\,d_1^3}\right) \quad (5)$$

Hence,

$$\frac{M_{II}}{M_{bs}} = \frac{32}{\pi\left(1-\frac{d_1^4}{d_y^4}\right)}\left(\frac{1}{6}-\frac{a^2}{3d_y^2}+\frac{a^4}{5\,d_y^4}+\frac{a^6}{3\,d_y^6}-\frac{d_1^3}{6\,d_y^3}+\frac{a^2d_1}{3\,d_y^3}+\frac{a^4}{5\,d_1d_y^3}-\frac{a^6}{3\,d_1^3d_y^3}\right) \quad (6)$$

Numerical values for the relationship between d_1/d_y and $p = M_I/M_{bs}$ and $p = M_{II}/M_{bs}$ are given in Table II, and is plotted in Fig. 6. It can be that for $d_1/d_y = 0$, it is $p = 1.33$, and for $d_1/d_y = 1$, it is $p = 1$. The common point for both M_I/M_{bs} and M_{II}/M_{bs} is given by $d_1/dy = 0.85$ and $p = 1.14$.

TABLE II.

	Case I : $0 < \frac{d_1}{d_y} < 8.05$ eq. 4. thick-walled tube							Case II : $0.85 < \frac{d_1}{d_y} < 1$ eq. 6	
$\frac{d_1}{d_y}$	0	0.4	0.6	0.7	0.8	0.85	0.9	0.95	1.0
p	1.33	1.32	1.27	1.23	1.18	1.14	1.09	1.05	1.0

TABLE I.

	Case I : $a > \frac{d_1}{2}$ eq. 1. thick-walled tube							Case II : $a < \frac{d_1}{2}$ eq. 2. thin-walled tube		
$\eta = \frac{r}{R} = \frac{d_1}{d_y}$	0	0.320	0.380	0.445	0.652	0.775	0.850	0.900	0.950	1.0
$\xi = \frac{a}{R} = 2\,\frac{a}{d_y}$	0.686	0.687	0.690	0.700	0.750	0.800	0.850	0.873	0.894	0.920

The point which defines the transition to full plastic behaviour throughout the sectional area is termed the bending-yield point or bs-limit, the corresponding apparent extreme fibre stress being σ'_s.

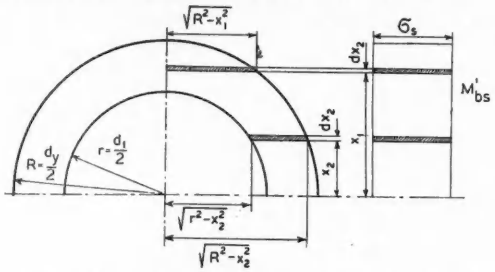

Fig. 7. **Bending-yield point for thick and thin-walled tubes.**

Referring to Fig. 7, the bending moment for the tube can be expressed by

$$M'_{bs}=4\,\sigma_s\left\{\int_r^R \sqrt{R^2-x_1^2}\,.\,x_1\,dx_1+\int_0^r \sqrt{R^2-x_2^2}-\sqrt{r^2-x_2^2}\,x_2\,dx_2\right\}$$

which gives

$$M'_{bs}=\frac{4\,\sigma_s}{3}(R_3-r_3) \text{ or } M'_{bs}=\frac{\sigma_s}{6}(d_y^3-d_1^3) \quad (7)$$

The ratio of M'_{bs} to M_{bs} is denoted s, and can be expressed as

$$s=\frac{M'_{bs}}{M_{bs}}=\frac{\sigma'_s}{\sigma_s}=\frac{16}{3\pi}\cdot\frac{1-\left(\frac{d_1}{d_y}\right)^3}{1-\left(\frac{d_1}{d_y}\right)^4} \quad .. \quad (8)$$

Numerical values for this relationship are given in Table III, and the corresponding curve is plotted in Fig. 6. For a value of $d_1/d_y = 0$, it is $s = 1.7$, and for $d_1/d_y = 1$, an value of $s = 1.27$ results.

TABLE III.

$\frac{d_1}{d_y}$	0	0.2	0.4	0.6	0.7	0.8	0.9	1.0
s	1.7	1.68	1.63	1.54	1.48	1.41	1.34	1.27

The shaded area between the p and the s curves indicated in Fig. 6 represents the range within which the bending curve begins to deviate from a straight line for various ratios of inside and outside tube diameters, and takes the shape which corresponds to the full attainment of the yield point within the section.

INTERNAL SHOE BRAKES

By DIPL.-ING. HANS W. LINDEMANN, *VDI/ATG*, Braunschweig. (From *ATZ-Automobiltechnische Zeitschrift*, Vol. 46, No. 15/16, August, 1943, pp. 367-372).

CALCULATIONS of considerable accuracy which have been published so far assume a sinusoidal stress distribution over the brake lining. This is equivalent to the assumption that the brake lining is of uniform thickness and obeys Hook's law. Thus the stress in the lining

$$K=E\epsilon=E\frac{\Delta s}{s}=E\frac{b\,.\sin\beta\,.\,\delta}{s}=\varphi\,\delta\,b\sin\beta=K_1\sin\beta_1$$

where φ = E/s = constant,
E = modulus of elasticity,
s = thickness of lining,
δ = angular deflection of brake shoe resulting in stress
K_1 = a constant = k_{max},
β and b see Figs. 1, 2, etc.

The distribution of pressure depends on wear and the law of elasticity which determines the distortion of the lining. In the case of a brake which has been run in, the sinusoidal distribution of wear can be proved in the following way :—

Let the circle $X\,Y\,Z$ with center M (Fig. 1) represent the lining when it is new and the brakes are on, and also the circumference of the brake drum. During the whole life of the lining let M move to M', so that the

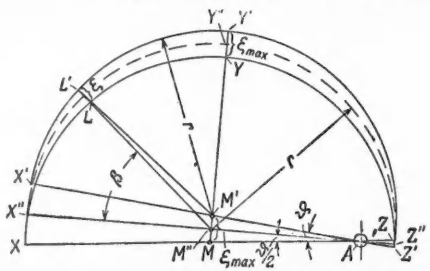

Fig. 1. **Wear of brake shoe.**

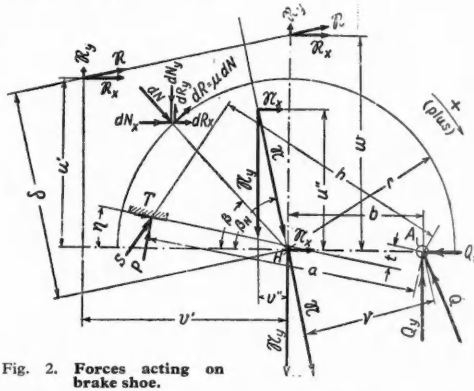

Fig. 2. **Forces acting on brake shoe.**

shoe rotates about the anchorage pin A through an angle ϑ. If the circle $X'\,Y'\,Z'$ with the center at M' and radius r be described, the distance between the two circles is the wear ζ. The maximum wear ζ_{max} is on the diameter MM'. If we draw $X''\,M''\,AZ''$ at right angles to MM' bisecting the angle ϑ, we obtain the following equation for any point L.

$$r^2=\left(r+\frac{\zeta}{2}\right)^2+\left(\frac{\zeta_{max}}{2}\right)^2-2\,\frac{r+\zeta}{2}\,\frac{\zeta_{max}}{2}\cos(90-\beta).$$

From this we get

$$\zeta=\zeta_{max}\sin\beta-R,$$

where

$$R=2r\left[1-\sqrt{1-\left(\frac{\zeta_{max}}{2r}\cos\beta\right)^2}\right]$$

$$=2r\left[\frac{1}{2}\left(\frac{\zeta_{max}}{2r}\cos\beta\right)^2+\ldots\right]=\frac{\zeta^2_{max}\cos^2\beta}{4r}$$

when $\beta = 90$ deg., then $R = 0$, which agrees with the sinusoidal law.

when $\beta = 0$ deg., then $R = \dfrac{\zeta^2_{max}}{4r}$,

when e.g. $\zeta_{max} = 6$ mm., $r = 200$ mm., then $R = 0.045$ mm.

$$\frac{R}{\zeta_{max}} \cdot 100 = \frac{0.045}{6} \cdot 100 = 0.75 \text{ per cent.}$$

which obviously can be neglected, so that

$$\zeta = \zeta_{max} \sin \beta \quad .. \quad .. \quad .. \quad (2)$$

Examining the conditions of pressure the following relationship between pressure and wear is obtained

$$\frac{d\zeta}{dT} = \left(\frac{k v}{60 \times 75}\right) \vartheta \quad .. \quad .. \quad (3)$$

where $d\zeta$ = increment of wear in cm.
dT = increment of time in min.
kv = frictional power in kgm/cm²sec.
ϑ = coefficient of wear in cm³/H.P. hr.

The coefficient of wear determines the quality of the lining material and varies with its temperature. This can be expressed by the equation

$$\vartheta = \frac{e^{t/100}}{23.25} \quad .. \quad .. \quad .. \quad (4)$$

where t is in deg. C., and $e = 2.718$. It must be, therefore, assumed that the temperature at any point of the lining is the same and this is approximately true.

As v is constant over the whole circumference the following equation can be obtained for the center part YY' (Fig. 1) and an arbitrary point LL' on the lining by means of equations (2) and (3).

$$\frac{k}{k_{max}} = \frac{d\zeta}{d\zeta_{max}} = \sin \beta \quad .. \quad .. \quad (5)$$

This equation of the sinusoidal distribution of pressure is valid for any law of elasticity, such as e.g.,

$$k = K(e^{C\epsilon} - 1) \quad .. \quad .. \quad (6)$$

where $\epsilon = \dfrac{ds}{s}$ is the strain corresponding to the pressure k, K *and* C being constants.

By altering the brake load (force at expander cam) the distribution of pressure is altered because of the elastic deformation of the lining. When the load remains constant running in again takes place according to a sinusoidal law. In practice, however, constant conditions cannot be obtained, the brake load being constantly changed. The sinusoidal law and the state of running in can be related to a mean brake load only.

RESULTANT FORCES AT THE LEADING AND TRAILING SHOE.

The knowledge of the resultant is not required for the determination of the brake effects. The main equations can always be stated by means of the differentials of the forces. The constants of the brake shoe (Table 1) and " self-energising factor "

$$f = \frac{1}{1 \,(\mp)\, \mu \left(\dfrac{A}{B} + \dfrac{rE}{bB}\right)} \quad .. \quad .. \quad (7)$$

are extremely useful in calculations.

Below, all equations are stated to clarify any doubts arising from existing literature; vectors (Fig. 2) are indicated by German type.

(*a*) *Differentials of forces.*

$$dN = k z r \, d\beta = z r K_1 \sin \beta \, d\beta = K_2 \sin \beta \, d\beta \quad .. \quad (8)$$

where z = width of lining, $K_2 = z r K_1$ = constant

$$\left.\begin{aligned} dR &= \mu \, dN = \mu K_2 \sin \beta \, d\beta && (9)\\ dN_x &= dN \cos \beta = K_2 \sin \beta \cos \beta \, d\beta && (10)\\ dN_y &= dN \sin \beta = K_2 \sin^2 \beta \, d\beta && (11)\\ dR_x &= dR \sin \beta = \mu K_2 \sin^2 \beta \, d\beta && (12)\\ dR_y &= dR \cos \beta = \mu K_2 \sin \beta \cos \beta \, d\beta && (13) \end{aligned}\right\} \; tg\,\beta = \frac{dN_y}{dN_x} = \frac{dR_x}{dR_y} \quad (14)$$

(*b*) *Linear sum of forces for the determination of the braking torque.*

$$\text{Normal forces } N = \int_{\beta_1}^{\beta_2} dN = K_2 \int_{\beta_1}^{\beta_2} \sin \beta \, d\beta = K_2 E \quad (15)$$

$$\text{Circumferential forces } U = \int_{\beta_1}^{\beta_2} \mu \, dN = \mu K_2 \int_{\beta_1}^{\beta_2} \sin \beta \, d\beta = \mu K_2 E \quad (16)$$

(*c*) *Vectorial resultant.*

$$\mathfrak{N}_x = \mathfrak{N} \cos \beta_N = K_2 \int_{\beta_1}^{\beta_2} \sin \beta \, \cos \beta \, d\beta = K_2 A \quad (17)$$

$$\mathfrak{N}_y = \mathfrak{N} \sin \beta_N = K_2 \int_{\beta_1}^{\beta_2} \sin^2 \beta \, d\beta = K_2 B \quad .. \quad (18)$$

$$\mathfrak{N} = \sqrt{\mathfrak{N}_x^2 + \mathfrak{N}_y^2} = K_2 \sqrt{A^2 + B^2} \quad .. \quad (19)$$

$$\mathfrak{R}_x = \mathfrak{R} \sin \beta_N = \mu K_2 \int_{\beta_1}^{\beta_2} \sin^2 \beta \, d\beta = K_2 B \quad .. \quad (20)$$

$$\mathfrak{R}_y = \mathfrak{R} \cos \beta_N = \mu K_2 \int_{\beta_1}^{\beta_2} \sin \beta \cos \beta \, d\beta = \mu K_2 A \quad (21)$$

$$\mathfrak{R} = \sqrt{\mathfrak{R}_x^2 + \mathfrak{R}_y^2} = \mu K_2 \sqrt{A^2 + B^2} = \mu \mathfrak{N} \quad (22)$$

$$\text{tg } \beta_N = \frac{\mathfrak{N}_y}{\mathfrak{N}_x} = \frac{\mathfrak{R}_x}{\mathfrak{R}_y} = \frac{B}{A} \quad .. \quad .. \quad (23)$$

$$\sin \beta_N = \frac{\mathfrak{N}_y}{\mathfrak{N}} = \frac{B}{\sqrt{A^2+B^2}} \quad .. \quad .. \quad (24)$$

$$\cos \beta_N = \frac{\mathfrak{N}_x}{\mathfrak{N}} = \frac{A}{\sqrt{A^2+B^2}} \quad .. \quad .. \quad (25)$$

(*d*) *Position and Direction of Resultant.*

The integral over the whole lining angle of the moments of the differentials of the forces about the anchorage pin A must be equal to the moment of the resultant about the point A (Fig. 2).

$$\mathfrak{R}_x u' = \int_{\beta_1}^{\beta_2} dR_x \, r \sin \beta$$

$$u' = r \frac{\displaystyle\int_{\beta_1}^{\beta_2} \sin^3 \beta \, d\beta}{\displaystyle\int_{\beta_1}^{\beta_2} \sin^2 \beta \, d\beta} = r \frac{H}{B} \quad .. \quad (26$$

$$\mathfrak{R}_y (b + v') = \int_{\beta_1}^{\beta_2} dR_y (b + r \cos \beta)$$

$$v' = r\,\frac{\int_{\beta_1}^{\beta_2} \sin\beta\cos^2\beta\,d\beta}{\int_{\beta_1}^{\beta_2} \sin\beta\cos\beta\,d\beta} = r\,\frac{G}{A} \qquad (27)$$

$$\mathfrak{R}\rho = \int_{\beta_1}^{\beta_2} r\,dR$$

$$\rho = r\,\frac{E}{\sqrt{A^2+B^2}} \quad .. \quad .. \quad .. \qquad (28)$$

If $\mathfrak{R}$ is shifted to the y-axis and resolved into its components then the distance of $\mathfrak{R}_x$ from the x-axis

$$w = \frac{\rho}{\sin\beta_N} = \rho\,\frac{\mathfrak{R}}{\mathfrak{R}_y} = r\,\frac{E}{B} \quad .. \quad .. \qquad (29)$$

$$\mathfrak{R}_x\,u'' = \int_{\beta_1}^{\beta_2} d\,N_x\,r\sin\beta$$

$$u'' = r\,\frac{\int_{\beta_1}^{\beta_2} \sin^2\beta\cos\beta\,d\beta}{\int_{\beta_1}^{\beta_2} \sin\beta\cos\beta\,d\beta} = r\,\frac{F}{A} \qquad (30)$$

$$\mathfrak{R}_y\,(b+v'') = \int_{\beta_1}^{\beta_2} d\,N_y\,(b + r\cos\beta)$$

$$v'' = r\,\frac{\int_{\beta_1}^{\beta_2} \sin^2\beta\cos\beta\,d\beta}{\int_{\beta_1}^{\beta_2} \sin^2\beta\,d\beta} = r\,\frac{F}{B} \qquad (31)$$

$$v = b\sin\beta_N = b\,\frac{\mathfrak{R}_y}{\mathfrak{R}} = b\,\frac{B}{\sqrt{A^2+B^2}} \quad .. \qquad (32)$$

$$\tan\beta_N = \frac{v'}{w-u'} = \frac{u''}{v''} = \frac{B}{A} \quad .. \qquad (33)$$

which agrees with equation (23). It also follows that $\mathfrak{R}$ is perpendicular to $\mathfrak{A}$, and that $\mathfrak{A}$ passes through the center M.

In deducing equation (33) it should be borne in mind that

$$\int_{\beta_1}^{\beta_2} \sin\beta\,d\beta - \int_{\beta_1}^{\beta_2} \sin^3\beta\,d\beta = \int_{\beta_1}^{\beta_2} \sin\beta\cos^2\beta\,d\beta$$

or $$E = G + H \quad .. \quad .. \quad .. \qquad (34)$$

Furthermore it should be noted that with leading and trailing shoes the position of the resultant depends only on the masses, but is independent of the direction of rotation, the frictional coefficient, the braking effect, and the magnitude of the transmitted forces. The magnitude and direction of $\mathfrak{R}$ changes with the direction of rotation.

(e) *Symmetrical brake shoes.*

When the brake lining is symmetrical ($\beta_2 = 180$ deg.$-\beta_1$) we get (Fig 4.)

$A, D, F, v'', \mathfrak{R}_x, \mathfrak{R}_y = 0$ (35) $\quad v' = \infty$ (38)

$B, C, E, G, H, u' > 0$ (36) $\quad \rho = w = r\,\frac{E}{B}$ (39)

$\beta_N = 90$ deg. and $\tan\beta_N = \infty$ (37) $\quad v = b$

$$u'' = r\,\frac{F}{A} = \frac{0}{0} = \text{indeterminate} = r\,\frac{\int_{\beta_1}^{\beta_2} \sin^2\beta\cos\beta\,d\beta}{\int_{\beta_1}^{\beta_2} \sin\beta\cos\beta\,d\beta} =$$

$$= \frac{2}{3}\,r\,\frac{\sin^3\beta_2 - \sin^3\beta_1}{\sin^2\beta_2 - \sin^2\beta_1} =$$

$$= \frac{2}{3}\,r\,\frac{(\sin\beta_2 - \sin\beta_1)(\sin^2\beta_2 + \sin\beta_2\sin\beta_1 + \sin^2\beta_1)}{(\sin\beta_2 - \sin\beta_1)(\sin\beta_2 + \sin\beta_1)}$$

$$= \frac{2}{3}\,r\,\frac{3\sin^2\beta_1}{2\sin\beta_1} = r\sin\beta_1 > 0 \quad .. \quad .. \quad .. \qquad (40)$$

$$\mathfrak{R}_y\,(b+v') = 0.\ \infty = \text{indeterminate} = \int_{\beta_1}^{\beta_2} d\,R_y\,(b + r\cos\beta)$$

$$= \mu\,K_2\,[b\int_{\beta_1}^{\beta_2} \sin\beta\cos\beta\,d\beta + r\int_{\beta_1}^{\beta_2} \sin\beta\cos^2\beta\,d\beta] =$$

$$= \mu\,K_2\,(b\,A + r\,G) = \mu\,K_2\,r\,G \quad .. \qquad (41)$$

as $A = 0$

$$\mathfrak{R} = \mu\,K_2\,B = \mathfrak{R}_x \quad .. \quad .. \qquad (42)$$

$$\mathfrak{R}\rho = \mathfrak{R}_y\,(b+v') + \mathfrak{R}_x\,u'$$

therefore $$\rho - u' = \frac{\mu\,K_2\,r\,G}{\mu\,K_2\,B} = r\,\frac{G}{B} \quad .. \qquad (43)$$

$$\mathfrak{R} = \mathfrak{R}_y \quad .. \quad .. \qquad (44)$$

Thus, $\rho = w$, but $\neq u'$. The resultant $\mathfrak{R}$ and its component $\mathfrak{R}_x$ are equal and parallel to the distance $\rho - u'$ which follows from equation (43). Both forces intersect at infinity. The distance of $\mathfrak{R}_y$ from A is also

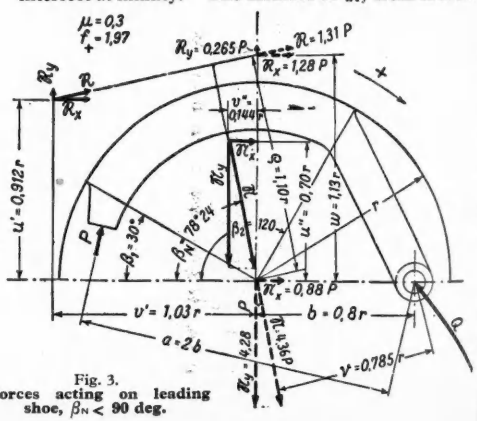

Fig. 3.
Forces acting on leading shoe, $\beta_N < 90$ deg.

$b + v' = \infty$. Although $\mathfrak{R}_y = 0$, the moment $\mathfrak{R}_y (b + v')$ according to equation (41) has a finite value; this is explained by the fact that $d\,\mathfrak{R}_y$ on the left and right side of the y-axis is of opposite direction.

(f) Unsymmetrical Brake Shoes.

When the braking surface is displaced towards the expander cam, i.e., when $\beta_2 < 180$ deg. — β_1 and $\beta_N < 90$ deg. (Fig. 3), then

$A, B, C, D, E, F, G, H, u', v', u'', v'', \rho, w, \nu, \tan\beta_N, \mathfrak{R}_x$, and $\mathfrak{R}_y > 0$

$$\mathfrak{R}_x, \mathfrak{R}_y \gtrless 0.$$

Similarly, when the braking surface is displaced towards the anchorage pin A, $\beta_2 > 180$ deg. — β_1, and $\beta_N > 90$ deg. (Fig. 5).

$$B, C, E, G, H, u', u'', \rho, w, \nu, \mathfrak{R}_y > 0$$
$$A, D, F, v' v'', \tan\beta_N, \mathfrak{R}_x < 0$$
$$\mathfrak{R}_x \gtrless 0 \qquad \mathfrak{R}_y \lessgtr 0.$$

MAIN EQUATION, EQUATION OF MOMENTS.

All forces are fixed if the constant K_2 which contains the angle δ is known, the constants of the brake shoe and the coefficient of friction μ being known values as they depend on the dimension of the brake shoe and the material of the lining respectively. K_2 depends on the force S at the expander cam (Fig. 2) and is determined by means of the equation of moments. Because of the complicated design of brakes it is recommended to resolve the force S into two components P perpendicular and T parallel to the surface in contact with the expander cam (Fig. 2). Then

$$S\,h = Pa - Tt \quad .. \quad .. \quad (45)$$

Thus the equation of moments can be expressed either as

$$Pa - Tt - \mathfrak{N}\nu(\pm)\,\mathfrak{R}\,(b\cos\beta_N + \rho) = 0 \quad .. \quad (46)$$

or as

$$Pa - Tt + \mathfrak{R}_x u'' - \mathfrak{R}_y (v'' + b)(\pm)\,\mathfrak{R}_x u'(\pm)\,\mathfrak{R}_y (v' + b) = 0 \quad .. \quad .. \quad .. \quad (47)$$

or as

$$Pa - Tt - \mathfrak{R}_y\, b\,(\pm)\,\mathfrak{R}_x\, w\,(\pm)\,\mathfrak{R}_y\, b = 0 \quad (48)$$

and using the values given in paragraphs 2 c and 2 d we get for each case

$$Pa - Tt = K_2\,[b\,B\,(\mp)\,\mu\,(b\,A + r\,E)] \quad .. \quad (49)$$

Solving equation (47) the finite value given by equation (41) has to be substituted for the inderterminate value of $\mathfrak{R}_y\,(v' + b)$.

The main equation (49) can be directly obtained without using vectorial resultants from

$$d\,Pa - d\,T\,t - dN\,b\sin\beta\,(\pm)\,\mu\,dN\,(b\cos\beta + r) = 0 \quad (50)$$

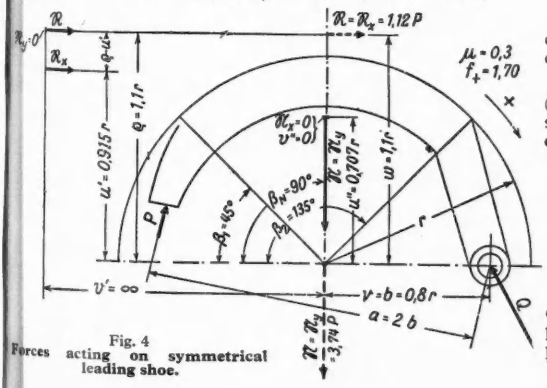

Fig. 4
Forces acting on symmetrical leading shoe.

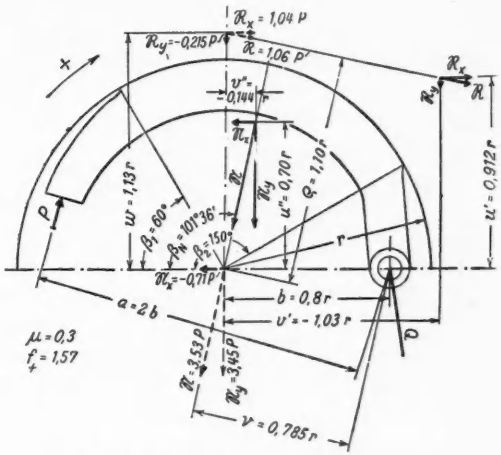

Fig. 5. **Forces acting on leading shoe, $\beta_N > 90$ deg.**

By means of the equations in paragraph 2a we obtain

$$P\,a - T\,t - \int_{\beta_1}^{\beta_2} K_2\,b\sin^2\beta\,d\beta\,(\pm)\int_{\beta_1}^{\beta^2}\mu\,K_2\,b\sin\beta\cos\beta\,d\beta$$
$$(\pm)\int_{\beta_1}^{\beta_2}\mu\,K_2\,r\sin\beta\,d\beta = 0 \quad .. \quad (51)$$

and on substituting the constants given in paragraph 6 we obtain the main equation (49).

From equations (15) and (49) the linear sum of the normal forces is obtained

$$N = K_2\,E = (P\,a - T\,t)\,\frac{E}{b\,B\,(\mp)\,\mu\,(b\,A + r\,E)} \quad .. \quad (52)$$

when $\mu = 0$, i.e., when the drum is stationary

$$N_0 = (P\,a - T\,t)\,\frac{E}{b\,B} \quad .. \quad .. \quad .. \quad (53)$$

and using equation (7)

$$N = N_0 f = (P\,a - T\,t)\,\frac{E}{b\,B}\,f \quad .. \quad .. \quad (54)$$

These equations prove to be very advantageous when calculations on brakes of complicated design are to be carried out.

The "self-energising" is positive for $1 < f < \infty$ (leading shoe), and negative for $1 > f > 0$ (trailing shoe). "Self-checking" we get for $f \longrightarrow \infty$ and $f < 0$ or

$$\mu\,\infty \geqq \frac{B}{A + \frac{r}{b}E} \quad .. \quad .. \quad .. \quad (55)$$

FORCES AT ANCHOR PIN AND BEARING.

To calculate these the vectorial resultants are required. In practice these calculations hardly ever are performed; the anchor pin is made specially stiff to prevent rattling and squeaking, and bearing designs are based on other factors.

The force on the anchorage pin (Fig. 2)

$$Q = \sqrt{Q_x^2 + Q_y^2} \quad .. \quad .. \quad (56)$$

where $Q_x = \mathfrak{R}_x\,(\pm)\,\mathfrak{R}_x + P \sin \eta + T \cos \eta$ (57)

and $Q_y = \mathfrak{R}_y\,(\mp)\,\mathfrak{R}_y - P \cos \eta + T \sin \eta$ (58)

further the force exerted on one side of the bearing

$$L = \sqrt{[(\mathfrak{R}_{y+} - \mathfrak{R}_{y+}) - (\mathfrak{R}_{y-} - \mathfrak{R}_{y-})]^2 + [(\mathfrak{R}_{x+} + \mathfrak{R}_{x+}) + (\mathfrak{R}_{x-} + \mathfrak{R}_{x-})]^2} \quad (59)$$

When substituting for the components of the forces the correct signs of the components are obtained from paragraph 2c.

BRAKE EFFECT

The factor w which is the ratio of the torque M_t exerted on the brake drum and the torque M_s exerted on the expander cam, is a suitable criterion for comparing different brake designs.

In the case of brakes without expander cam it is awkward to calculate M_s and thus to determine w. Here it is better to determine the factor λ obtained by dividing the total force acting at the circumference of the brake drum by the force exerted by the plunger or wedge respectively. Thus we have to distinguish between the torque criterion which in principle applies to any brake

$$w = \frac{M_t}{M_s} = \frac{r\,\Sigma\,U}{2\,n\,S} \quad (60)$$ where n is the radius of the expander cam, and the force criterion which is not applicable to brakes with rigidly mounted expander cams but can be used for wedge or hydraulically operated brakes.

$$\lambda = \frac{\Sigma\,U}{S} = 2\,w\,\frac{n}{r} \quad .. \quad .. \quad (61)$$

When $T = 0$, i.e., $S = P$, which is nearly always the case with brakes of the second kind

$$w = \frac{r\,\Sigma\,U}{2\,n\,P} = \frac{\mu\,r\,\Sigma\,N}{2\,n\,P} \quad .. \quad .. \quad (62$$

$$\lambda = \frac{\Sigma\,U}{P} = \frac{\mu\,\Sigma\,N}{P} \quad .. \quad .. \quad (63)$$

In this case the force exerted by the plunger

$$P = \frac{M_s}{2\,n} = \frac{M_t}{w\,2\,n} = \frac{M_t}{\lambda\,r} = \frac{r\,\Sigma\,U}{w\,2\,n} = \frac{\Sigma\,U}{\lambda} \quad (64)$$

The effect of the springs on the force exerted by the expander cam or the plunger has, of course, to be taken also into account.

BRAKE SHOE CONSTANTS.

The constants of brake shoes can be obtained by interpolation from Table I, which is generally valid. An example illustrating this is shown below.

The constants C and D are required for servo-brakes only, while constants F, G, and H are used for determining vectorial resultants. To determine the braking effect of ordinary brakes with two shoes the constants A, B, and E are sufficient.

Example :

$\beta_2 = 171.3°$	$A_2 = 0.012$	$B_2 = 1.569$	$E_2 = 0.988$
$\beta_1 = 52.3°$	$A_1 = 0.313$	$B_1 = 0.213$	$E_1 = 0.612$
Subtracting	$A = 0.301$	$B = 1.356$	$E = 1.600$

TABLE I. CONSTANTS OF BRAKE SHOES (INTEGRALS).

β	$A\beta$	$B\beta$	$C\beta$	$D\beta$	$E\beta$	$F\beta$	$G\beta$	$H\beta$
0	0	0	0	0	−1,000	0	−0,333	−0,667
2	0,002	0	0,035	0,035	−0,999	0	−0,332	−0,667
4	0,003	0	0,070	0,070	−0,998	0	−0,331	−0,667
6	0,006	0,001	0,104	0,105	−0,994	0	−0,327	−0,667
8	0,010	0,001	0,138	0,139	−0,990	0,001	−0,323	−0,667
10	0,015	0,002	0,172	0,174	−0,985	0,002	−0,319	−0,666
12	0,021	0,003	0,205	0,208	−0,978	0,003	−0,312	−0,666
14	0,029	0,005	0,238	0,242	−0,970	0,005	−0,304	−0,666
16	0,038	0,008	0,271	0,276	−0,961	0,007	−0,296	−0,665
18	0,048	0,011	0,303	0,309	−0,951	0,010	−0,287	−0,664
20	0,058	0,014	0,334	0,342	−0,940	0,013	−0,277	−0,663
22	0,070	0,018	0,364	0,375	−0,927	0,017	−0,266	−0,661
24	0,083	0,023	0,394	0,407	−0,913	0,022	−0,254	−0,659
26	0,096	0,029	0,423	0,438	−0,899	0,028	−0,242	−0,657
28	0,110	0,036	0,451	0,470	−0,883	0,034	−0,229	−0,654
30	0,125	0,044	0,478	0,500	−0,866	0,041	−0,216	−0,650
32	0,140	0,053	0,504	0,530	−0,848	0,049	−0,203	−0,645
34	0,156	0,064	0,529	0,559	−0,829	0,058	−0,190	−0,639
36	0,172	0,076	0,552	0,588	−0,809	0,068	−0,176	−0,633
38	0,189	0,088	0,574	0,616	−0,788	0,078	−0,163	−0,625
40	0,206	0,103	0,595	0,643	−0,766	0,089	−0,150	−0,616
42	0,223	0,119	0,615	0,669	−0,743	0,100	−0,137	−0,606
44	0,240	0,136	0,633	0,695	−0,719	0,112	−0,124	−0,595
46	0,258	0,153	0,650	0,719	−0,695	0,124	−0,112	−0,583
48	0,276	0,171	0,666	0,743	−0,669	0,137	−0,100	−0,569
50	0,293	0,190	0,681	0,766	−0,643	0,150	−0,088	−0,555
52	0,310	0,210	0,695	0,788	−0,616	0,163	−0,077	−0,539
54	0,327	0,232	0,709	0,809	−0,588	0,176	−0,067	−0,521
56	0,343	0,256	0,721	0,829	−0,559	0,190	−0,057	−0,502
58	0,359	0,281	0,731	0,848	−0,530	0,203	−0,048	−0,482
60	0,375	0,307	0,740	0,866	−0,500	0,216	−0,040	−0,460
62	0,390	0,334	0,748	0,883	−0,470	0,229	−0,033	−0,437
64	0,404	0,362	0,755	0,899	−0,438	0,242	−0,027	−0,411
66	0,417	0,390	0,761	0,913	−0,407	0,254	−0,021	−0,386
68	0,430	0,419	0,766	0,927	−0,375	0,266	−0,016	−0,359
70	0,442	0,449	0,771	0,940	−0,342	0,277	−0,012	−0,330
72	0,452	0,480	0,775	0,951	−0,309	0,287	−0,009	−0,300
74	0,462	0,512	0,778	0,961	−0,276	0,296	−0,006	−0,270
76	0,470	0,545	0,780	0,970	−0,242	0,304	−0,004	−0,238
78	0,478	0,579	0,782	0,978	−0,208	0,312	−0,003	−0,205
80	0,485	0,613	0,783	0,985	−0,174	0,319	−0,002	−0,172
82	0,491	0,647	0,784	0,990	−0,139	0,323	−0,001	−0,138
84	0,495	0,681	0,785	0,994	−0,105	0,327	−0,001	−0,104
86	0,498	0,715	0,785	0,998	−0,070	0,331	0	−0,070
88	0,499	0,750	0,785	0,999	−0,035	0,332	0	−0,035
90	0,500	0,785	0,785	1,000	0	0,333	0	0
92	0,499	0,820	0,785	0,999	0,035	0,332	0	0,035
94	0,498	0,855	0,785	0,998	0,070	0,331	0	0,070
96	0,495	0,890	0,785	0,994	0,105	0,327	0,001	0,104
98	0,491	0,925	0,786	0,990	0,139	0,323	0,001	0,138
100	0,485	0,959	0,788	0,985	0,174	0,319	0,002	0,172
102	0,478	0,993	0,788	0,978	0,208	0,312	0,003	0,205
104	0,470	1,026	0,790	0,970	0,242	0,304	0,004	0,238
106	0,462	1,058	0,793	0,961	0,276	0,296	0,006	0,270
108	0,452	1,089	0,796	0,951	0,309	0,287	0,009	0,300
110	0,442	1,120	0,800	0,940	0,342	0,277	0,012	0,330
112	0,430	1,150	0,805	0,927	0,375	0,266	0,016	0,359
114	0,417	1,181	0,810	0,913	0,407	0,254	0,021	0,386
116	0,404	1,209	0,816	0,899	0,438	0,242	0,027	0,411
118	0,390	1,238	0,823	0,883	0,470	0,229	0,033	0,437
120	0,375	1,265	0,831	0,866	0,500	0,216	0,040	0,460
122	0,359	1,290	0,840	0,848	0,530	0,203	0,048	0,482
124	0,343	1,341	0,850	0,829	0,559	0,190	0,057	0,502
126	0,327	1,337	0,862	0,809	0,588	0,176	0,067	0,521
128	0,310	1,359	0,875	0,788	0,616	0,163	0,077	0,539
130	0,293	1,380	0,889	0,766	0,643	0,150	0,088	0,555
132	0,276	1,400	0,904	0,743	0,669	0,137	0,100	0,569
134	0,258	1,419	0,920	0,719	0,695	0,124	0,112	0,583
136	0,240	1,436	0,937	0,695	0,719	0,112	0,124	0,595
138	0,223	1,452	0,956	0,669	0,743	0,100	0,137	0,606
140	0,206	1,467	0,976	0,643	0,766	0,089	0,150	0,616
142	0,189	1,481	0,997	0,616	0,788	0,078	0,163	0,625
144	0,172	1,494	1,019	0,588	0,809	0,068	0,176	0,633
146	0,156	1,505	1,042	0,559	0,829	0,058	0,190	0,639
148	0,140	1,515	1,066	0,530	0,848	0,049	0,203	0,645
150	0,125	1,524	1,092	0,500	0,866	0,041	0,216	0,650
152	0,110	1,532	1,119	0,470	0,883	0,034	0,229	0,654
154	0,096	1,539	1,147	0,438	0,899	0,028	0,242	0,657
156	0,083	1,546	1,176	0,407	0,913	0,022	0,254	0,659
158	0,070	1,552	1,206	0,375	0,927	0,017	0,266	0,661
160	0,058	1,557	1,236	0,342	0,940	0,013	0,277	0,663
162	0,048	1,561	1,267	0,309	0,951	0,010	0,287	0,664
164	0,038	1,564	1,299	0,276	0,961	0,007	0,296	0,665
166	0,029	1,566	1,331	0,242	0,970	0,005	0,304	0,666
168	0,021	1,568	1,364	0,208	0,978	0,003	0,312	0,666
170	0,015	1,568	1,397	0,174	0,985	0,002	0,319	0,666
172	0,010	1,569	1,431	0,139	0,990	0,001	0,323	0,667
174	0,006	1,570	1,466	0,105	0,994	0	0,327	0,667
176	0,003	1,571	1,501	0,070	0,998	0	0,331	0,667
178	0,002	1,571	1,536	0,035	0,999	0	0,332	0,667
180	0	1,571	1,571	0	1,000	0	0,333	0,667

Definitions of Constants :

$$A=\int_{\beta_1}^{\beta_2}\sin\beta\cos\beta\,d\beta=\frac{1}{2}(\sin^2\beta_2-\sin^2\beta_1)\qquad=A\beta_2-A\beta_1$$

$$B=\int_{\beta_1}^{\beta_2}\sin^2\beta\,d\beta=\left(\frac{\beta_2}{2}-\frac{\sin 2\beta_2}{4}\right)-\left(\frac{\beta_1}{2}-\frac{\sin 2\beta_1}{4}\right)=B\beta_2-B\beta_1$$

$$C=\int_{\beta_1}^{\beta_2}\cos^2\beta\,d\beta=\left(\frac{\beta_2}{2}+\frac{\sin 2\beta_2}{4}\right)-\left(\frac{\beta_1}{2}+\frac{\sin 2\beta_1}{4}\right)=C\beta_2-C\beta_1$$

$$D=\int_{\beta_1}^{\beta_2}\cos\beta\,d\beta=\sin\beta_2-\sin\beta_1\qquad=D\beta_2-D\beta_1$$

$$E=\int_{\beta_1}^{\beta_2}\sin\beta\,d\beta=\cos\beta_1-\cos\beta_2\qquad=E\beta_2-E\beta_1$$

$$F=\int_{\beta_1}^{\beta_2}\sin^2\beta\cos\beta\,d\beta=\frac{1}{3}(\sin^3\beta_2-\sin^3\beta_1)\qquad=F\beta_2-F\beta_1$$

$$G=\int_{\beta_1}^{\beta_2}\sin\beta\cos^2\beta\,d\beta=\frac{1}{3}(\cos^3\beta_1-\cos^3\beta_2)\qquad=G\beta_2-G\beta_1$$

$$H=\int_{\beta_1}^{\beta_2}\sin^3\beta\,d\beta\qquad=\frac{1}{3}[\cos a_1(2+\sin^2 a_1)-\cos a_2(2+\sin^2 a_2)]\qquad=H\beta_2-H\beta_1$$

INDUCTION FURNACES FOR MELTING METALS AND ALLOYS

By J. MINSSIEUX. (From *Bulletin de la Société Francaise des Électriciens*, Vol. 4, No. 33, January, 1944, pp. 12–19)

Two principal types of induction furnaces are distinguished, viz. :—

(1) Furnaces with closed magnetic circuit, usually termed *Low-Frequency Induction Furnaces*, operated mostly at 50 cycles per sec. or at a still lower frequency.

A furnace of this type resembles a transformer with its secondary winding formed by a circular channel of molten metal. The best known of this kind is the Ajax Wyatt furnace. Typical properties of this class of furnace are the following : The charge must be composed of molten metal and operation is continuous, only about 70 per cent of any one heat being poured, a fresh charge being added to the remaining 30 per cent. As the heat is developed in the metal in the melting channel, this metal is hotter than that in the crucible containing the bulk of the charge. Furnaces in this category are direct connected to a.c. mains and operate with a power factor of 0.7–0.8.

(2) Furnaces without magnetic circuit, i.e., *High-Frequency Coreless Induction Furnaces* are operated at frequencies ranging from 500 to 5,000 cycles per second. The operating principle is that of an air transformer, the charge being contained in a crucible arranged in the centre of the primary transformer coil. The diminution in permeability caused by the absence of an iron core is to a certain extent compensated for by the increased operating frequency. Characteristic features of this type are : The cold charge received by the crucible is composed entirely of solid material of whatever shape is convenient, and the furnace is started from cold. There are difficulties in operating this furnace as a batch-type unit, particularly as the refractory lining is small in bulk. Heat is developed throughout the charge, or in any event along the entire periphery, so that the temperature of the refractory lining is not much different from that of the molten metal. A strong stirring action is induced by the electrodynamic effect. Lastly, a motor-generator set is required for the supply of the high-frequency current.

The following is intended as a brief survey of foundry practice, assuming that induction type furnaces are used for the various processes considered :

NON-FERROUS ALLOYS.

Copper alloys. In view of the large quantities produced, the furnace is kept in continuous operation for long periods without any change in the composition of the alloy. Since the melting point of the metal approximates to 900 deg. C., the maintenace of the refractory lining is an easy matter. Experience has shown that the low-frequency induction furnace is particularly suitable for this purpose and is due to the fact that the facility of temperature control afforded by this type of furnace makes it possible to keep melting losses down to about 1 per cent as compared to the 3–5 per cent loss incurred in fuel burning furnaces. Other advantages of the low-frequency furnace are saving in labour and the long service life of the refractory lining, one lining being good for the production of some 1,000 tons. The power consumption amounts to 200–240 kWhrs. per ton.

Bronze. In small foundries where frequent changes in the composition of the alloy are required, the low-frequency induction furnace cannot give satisfaction. Furthermore, the high temperature—up to 1250 deg. C.—required in the making of small bronze castings, requires a special refractory lining. These difficulties do not, however, exist in large bronze foundries turning out valves and fittings in continuous production without requiring any change in the composition. Thus, for instance, a bronze with 85 per cent copper and 9 per cent lead for valve bodies is produced in the low-frequency furnace with a consumption of 280–300 kWhrs. per ton, the refractory lining lasting some 6 months in continuous operation.

For intermittent production, high-frequency furnaces prove useful as changes in composition are easily effected, but the capital charges of this furnace type are too high for small foundries. High-frequency furnaces are, however, essential for the making of aluminium bronze because of the high melting point of this material and the oxidability of the aluminium. The power consumption approximates to abt. 450 kWhrs. per tons.

Pure Copper. When using low-frequency furnaces for the melting of pure copper, care must be taken to select a refractory lining capable of withstanding the corrosive action of the rapidly circulating metal. Approximately 300 kWhrs. are required per ton of metal. High-frequency furnaces can also be employed. While maintenace of the refractory lining is more favourable with this type of furnace, its efficiency is lower, as it depends on the relationship of the resistances of primary and secondary circuits, which in this application are both of copper.

Light alloys. In the melting of light alloys, their low melting point is a favourable factor. However, these alloys are easily oxidised and their melting requires a relatively high amount of electrical energy because of their high specific heat. When using low-frequency furnaces, the formation of oxides tends to obstruct the melting channel. This difficulty must be overcome by special measures such as the provision of special clean-

out holes, and the cleaning has to be carried out at regular intervals. On the other hand, low-frequency furnaces yield a highly homogeneous product; also their melting losses are low and amount to only 0.8 per cent as compared to 1.2 per cent with resistance furnaces and 1.5 per cent with oil-fired furnaces. This reduction in melting loss is due to the small amount of metal surface exposed to the air in induction type furnaces. The power consumption of the low-frequency furnace is some 500 kWhrs. per ton of light alloy as compared to 700 kWhrs. with the electrical resistance furnace.

Because of its cylindrical crucible the high-frequency furnace would appear to be free from the difficulties experienced with the melting channel of the low-frequency type. That this is not so is due to the fact that the bath agitation of light metal alloys may easily assume excessive proportions. This may be avoided by having recourse to very high frequencies generated by thermionic valves, but installations of this kind suffer from the disadvantage of high cost and comparatively low efficiency. Another solution would lie in the use of metallic crucibles in which the greater part of the induced currents is concentrated, thereby diminishing bath agitation by electrodynamic effects. The drawback of the procedure is the possible introduction of metallurgical interaction between the crucible and its contents.

Zinc. Low-frequency furnaces are highly suitable for the melting of zinc provided an appropriate refractory lining is used. Melting losses will not exceed 0.25 per cent and the power consumption will only amount to some 90–100 kWhrs. per ton of metal.

Precious Metals. Generally, the small quantities of precious metals to be handled do not justify the use of low-frequency furnaces. But the melting of silver or gold alloys in the crucible of the high-frequency furnace gives excellent results. Also, this type of furnace constitutes the only means for producing the high temperatures required for the melting of platinum (approx. 1800 deg. C.) and iridium (approx. 2200 deg. C.). Thus, for instance, a high-frequency furnace of 10–20 kW capacity will melt a charge of 2–3 kg. of platinum within 15 to 20 minutes.

NICKEL AND NICKEL ALLOYS.

German Silver. In the melting of German silver the low-frequency furnace exhibits all the advantages obtained with its employment for the melting of brass. However, in the case of German silver with its higher melting point, the danger of the loss of zinc from the alloy becomes more serious. Exact temperature control and uniformity of the heating effect must therefore be aimed at. The power consumption may be expected to range from 300 to 350 kWhrs. per ton. High-frequency furnaces can also be used, but their power consumption is some 400 kWhrs. per ton.

Cupro-nickel. Cupro-nickel alloys with nickel contents ranging from 25 to 45 per cent possess higher melting points than German silver. From the aspect of refractory service life, the employment of high-frequency furnaces will be preferred.

Nickel-chromium alloys. Large quantities of nickel-chromium alloy are required for the manufacture of electrical heating elements, the most commonly used composition containing 80 per cent nickel and 20 per cent chromium. Their production is carried out in high-frequency furnaces.

Pure nickel. The melting of pure nickel is commonly carried out in high-frequency furnaces of 200–500 kg. capacity. About 700 kWhrs. are required per ton of metal, melting times ranging from 1 to 2 hours.

FERROUS ALLOYS.

Cast iron. Present-day practice is concerned with producing a quality of cast iron the mechanical characteristics of which approximate to that of steel. More often than not this result is achieved with the help of an electric melting furnace. Where continuous production is involved the low-frequency induction furnace would appear as particularly suitable. Excellent efficiencies can be obtained with the Ajax Wyatt furnace, but the high temperature of 1500–1600 deg. C. required unduly shortens the service life of its melting channel. This difficulty, however, is absent from the high-frequency induction furnace equipped with crucible. This type of furnace is also used for carrying out the second stage of duplex-processes. Compared with the arc furnace the high-frequency furnace is higher in first cost, but the absence of electrodes and the smaller power consumption afford economy of operation.

The high-frequency furnace is also used for the production of certain special grades of cast iron such as heat-resisting or acid-resisting material. The power consumption will range from 600–700 kWhrs. per ton. Intermittent operation is possible. Another advantage is the very small loss in alloying elements.

Steels. For reasons stated above, the employment of low-frequency furnaces for steel making cannot be considered. Steel making is the proper domain of the high-frequency induction furnace. The similarity between the latter and the coke- or gas-fired crucible furnace is self-evident. For the past 150 years crucible furnaces were employed for high grade steel. Today, they are superseded by the high-frequency induction furnace for the following reasons :—

Individual heats may amount to several tons in weight as compared with a capacity of 40 to 50 kg. per individual crucible. Labour requirements are greatly reduced, particularly as the difficult handling of the crucibles is eliminated. Melting takes place with the exclusion of air and all possible sources of contamination are eliminated. In addition to the production of normal crucible steels, such as carbon tool steels, high-speed tool steels, or magnet steels, the high-frequency induction furnace also finds application in the making of chrome-nickel steels for armour plate and projectiles, and of stainless steel of the 18–8 type. A few data on typical up-to-date high-frequency furnace installations :

Furnace capacity, kg.	Power input (high frequency side), kW	Frequency cycles.	Time per heat, hr.	Power consumption per ton of steel, kWhr.
250	150	2,200	1	600–800
500	150	1,000	2½	600–800
500	300	1,000	1	600–750
1,000	300	1,000	2½	575–750
2,000	400	1,000	2⅝	550–700
5,000	1,250	1,000	3	530–700

The high-frequency furnace has also proved its worth in the making of steel castings, the product being greatly superior in quality to anything that could be achieved in previous practice. Other noteworthy advantages of the high-frequency furnace are the possibility of intermittent production, and the ease with which the very high temperature required for the casting of small pieces can be obtained. Most frequently the acid process is used because of the better casting properties of the metal so prepared. Compared with the electric arc furnace, the high-frequency induction furnace offers the advantages of smaller power consumption and of saving refractory material.

In order to increase the stirring action, double-frequency furnaces have been developed, the higher frequency mainly serving to melt the charge and the lower frequency to produce a strong motion of the bath.

MEASUREMENTS ON PLASMA DIFFUSION IN MERCURY ARCS

By ING J. IBL, Prague. (From *Elektrotechnicky Obzor*, Prague, Vol. 31, No. 7, July, 1942, pp. 97–103).

THE plasma of mercury vapour arcs is also diffused to parts of the vessel (e.g. a mercury arc rectifier), where there are no ignition electrodes. The properties of these "outer regions" of the arc, mainly the concentration of its plasma, are of paramount importance for the layout of mercury-arc-rectifiers, in particular so far as the control grids; the length of the anode shields; and the shape of the arms are concerned. Moreover, the concentration of the plasma limits the use of de-ionizing surfaces.

The conditions in the diffusing plasma, according to the author, are not yet experimentally investigated, though corresponding investigations for the arc proper have been carried out successfully by Langmuir.

The concentration of electrons and ions in parts of the vessel at a distance from the arc is a function of the pressure of the mercury vapour; of the shape of the vessel in these parts; the distance of the point under investigation from the core of the arc, and of the concentration of the arc. The plasma diffuses to the un-ignited parts of the vessel (e.g. to the arms of a mercury-rectifier) as shown theoretically by the following equation:

$$n = n_o \cdot e^{-\left[\frac{20.5}{\sqrt{A}}\sqrt{\frac{O}{F.al}}\sqrt{\frac{T_i}{T_e}}\right]x} \quad .. \quad (1)$$

In this equation:—

- n number of electrons or ions in one cm.^{3}, i.e. the concentration of the plasma at a given point.
- n_o concentration of the plasma at the mouth of the tank.
- e base of the system of natural logarithms.
- A ratio of the accidental density of the electron current and of the ion current at the point under investigation. This ratio is between 300 to 400.
- O circumference of the cylindrical part of the tank.
- F cross sectional area of the cylindrical part of the tank.
- a factor to allow for variations in the mean free path of elements between collisions; approximately 0.5 to 1.
- l mean free path of the elements (cm.).
- T_i temperature of the ions. It is assumed that the relations derived from Maxwell's speed distribution are applicable to this case (deg.K).
- T_e temperature of the electrons (deg.K).
- x distance between the investigated point and the point n_o.

This equation is valid for any cylinder of constant diameter provided that A is neither a function of n nor of x, and that T_i is much smaller than T_e. According to equation (1) the concentration of the plasma decreases more rapidly if O/F is large, which is the case if the cross section of the arm is subdivided by de-ionising grid. It also decreases more rapidly if the mean free path of the elements decreases. At higher temperatures of the vessel—with a corresponding rapid increase of the vapour pressure and a rapid decrease of l—a much smaller concentration at a given point may be expected, if compared with the concentration at a lower temperature.

A series of measurements were carried out to investigate the limits of the validity of equation (1), and also to determine other characteristics of the diffusing plasma of the electric arc. The vessel used for the experiments is shown in Fig. 1. It contains a cathode, an auxiliary anode nearby, and a number of small collecting electrodes. Vacuum was maintained below 0.0001 mm. Hg.-column by continuous pumping. The whole surface of the tank was water-cooled and the quantity of water circulating between the double walls was always adequate to maintain the Hg-vapour saturated at any point within the tank, except for the irregularities due to the dynamic pressure of the evaporating mercury on the cathode.

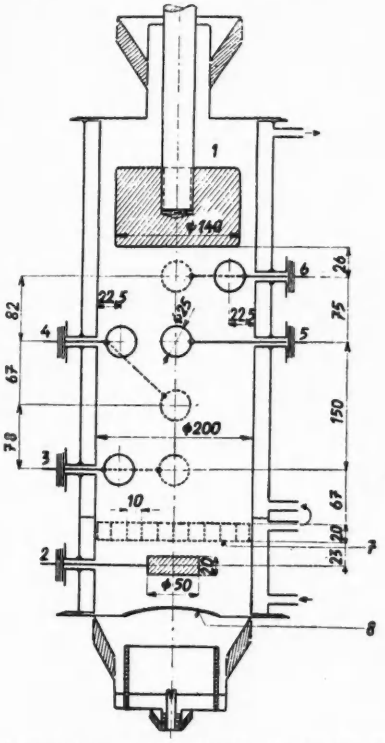

Fig. 1. **Schematic cross section through the vessel used for the experiments.**

1: graphite anode
2: graphite auxiliary anode
3-6: flat collecting electrodes, 25 mm. dia., 0.5 mm. thick; 10 cm.^{2} area
7: grid
8: iron sheet to limit the direct radiation from the cathode

THE MEASUREMENT.

A one-directional arc was maintained between the cathode and the auxiliary anode and the "characteristic data" of the plasma spreading from this auxiliary arc to the upper parts of the tank were found by measuring the corresponding values on the collecting electrodes. The measurements were carried out for various intensities of the auxiliary arc and at various temperatures of the cooling water. The electrical connections for these experiments are shown in Fig. 2, and the result of one actual series of measurements is given in Fig. 3. The volt-ampere characteristic of the collector was found by applying a variable voltage (with respect to the cathode) and by measuring the intensity of the current flowing from the cathode to the collector or vice-versa.

The ion-current flowing from the negative collector (Fig. 3), varies with the applied voltage only as long as the thickness, and thus the area at the outside of the

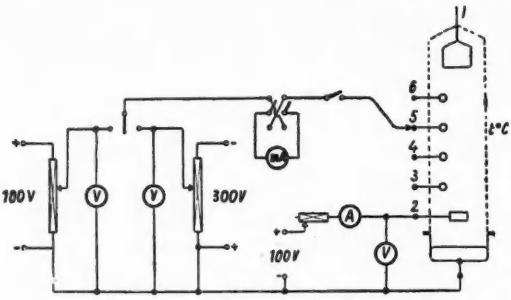

Fig. 2. **Connection diagram.**

sheath of ions built up around the collector, increases. When the voltage of the collector becomes much lower than that of the plasma, the increasing rate of afflux of electrons rapidly reduces the resultant current flowing from the collector, until finally the electron current exceeds the ion-current. At this point the curve representing the current of the collector shows a sharp turn, the current changes direction and its intensity increases to a multiple of its former value. Analysis of the curve made from data given is carried out in the following way: By extending the slightly inclined straight line part beyond the knee of the curve (caused by the electron current), the values for the electron and ion currents are separated. The pure electron current, plotted in a logarithmic scale (Fig. 3b) should be a straight line if the difference of potential of the collector is more negative than that of the plasma. The slope of the line indicates the temperature of the electrons. The fact that the line is straight confirms the Maxwellian theory of the speed of electrons. If the voltage of the collector is increased above that of the plasma, the curve forms a knee and the electron current continues to be only slightly influenced. This is explained by the fact that a sheath of electrons is formed around the collector, similar to the sheath of ions formed if the voltage of the collector is negative.

By examination of the curves, plotted from the measurements, the following properties of the plasma in the vicinity of the collector can be derived:

The potential V_p of the plasma,
The electron current i_e in the plasma at this point,
The ion-current i_j in the plasma at this point,
The temperature T_e of the electrons.

The author then gives the results of a series of experiments which he analyses in a number of graphs and tables.

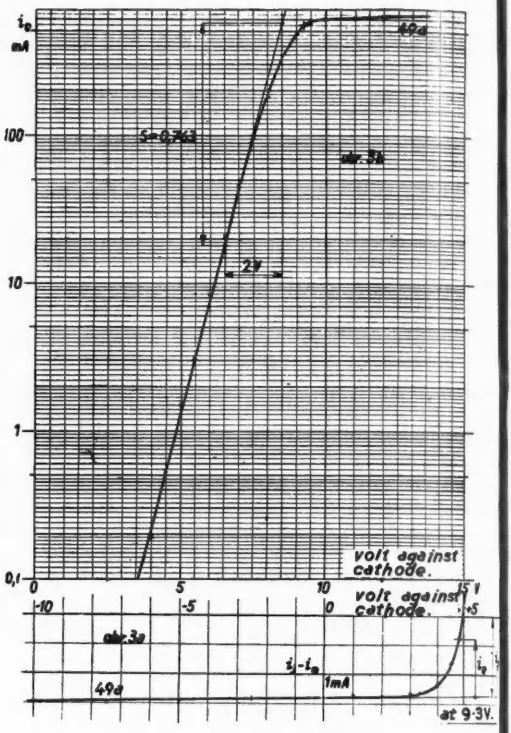

Fig. 3. **Sample measurement.**

Connected: collecting electrode No. 3; i_2 = 49A, t = 47.7/49.3 deg. C,
E^2 = 14 V, E_n = 5.1 V.
The measurement gave the following results:
V_p = 9.3 V
i_e = 550 mA — Ie = 5.5 × 10^{-2} A/cm.²
i_j = 1.36mA — Ij = 0.13 × 10^{-3} A/cm²
T_e = 11600/0.763 = 15200 deg. K.
$A = i_e/i_j$ = 404

$$n_e = \frac{4.04 \cdot 10^{13} \cdot Ie}{\sqrt{T_e}} = 1.78 \times 10^{10} \text{ electrons/cm.}^3$$

CO-ORDINATION OF INSULATION IN HIGH-TENSION PLANTS

By Ing. Sigurd Rump. (From *Elektroteknik, Ingenioren*, Copenhagen, No. 77, 13th November, 1943, pp. 149–161).

It is a well known fact, that in high-tension plants flash-over may be caused by overvoltages. In order to preclude damage to valuable machinery and apparatus, the insulation level should be so adjusted that the unavoidable flash-over can take place through the air, that is, at a point where its occurrence is harmless, thus minimising operating trouble and costly repairs. This requirement, which is by no means new, can be met by introducing a spark-gap without series resistance and with lower flash-over point than the other parts of the installation. In order to solve the problem in an economically justifiable manner, that is, without having to use over-dimensioned insulators whenever flash-over is to be expected, the following data must be ascertained:

(1) Magnitude and time-characteristics of over-voltages occurring during operation.
(2) The insulation level of machine, transformer, etc., insulation.
(3) The flash-over characteristic of the spark-gap.

While these data can be established on the basis of actual measurements, the following points must also be considered:

(4) Is it possible to utilise the available insulation to a higher degree than heretofore, thus raising operational safety without increased cost of installation?
(5) Which type of spark-gap is best suited, and will its operation have an adverse effect upon safety of plant operation?
(6) Can the effect of lightning strokes be prevented by other means than with the use of a spark-gap which has a lower flash-over voltage than the other parts of the installation concerned?

OVERVOLTAGES DUE TO EARTH FAULTS.

Reports available in literature show that voltages due to earth faults can be rendered harmless by reducing them to less than twice the line voltage by earthing the neutral or by the use of earth fault neutraliser coils. Overvoltages due to switching operations, as they may occur in de-energising long transmission lines, or in disconnecting unloaded transformers, etc., can be reduced by incorporating resistors in the breakers. This procedure must be considered as more economical than a general increase in the insulation level of the installation, particularly as in certain cases voltage surges due to circuit interruption may occur under very awkward conditions. For three-phase industrial networks the maximum voltage surges arising from switching operations can be taken as follows :

Operating Voltage	10	20	30	50	>50
Maximum Voltage / Times normal crest					
Between phases	4.7	3.9	3.2	2.5	<2.5
To earth	3.5	3.0	2.6	2.5	<2.5

Voltage surges due to earth faults or switching operations generally are of short duration, lasting less than 1/100 sec. Overvoltages due to atmospheric conditions are independent of the operating voltage but have an upper limit which is set by the insulation level of the installation concerned. They vary greatly in magnitude, and smaller surges are more frequent than larger ones. Therefore disturbances due to atmospheric influences are more frequent in installations operating at low voltage and having correspondingly weaker insulation than in networks operating at higher voltages and possessing a higher insulation level. For this reason, atmospheric disturbances in 15–30 kV systems are 4–5 times as frequent as in 60–100 kV installations.

Overvoltages caused by indirect lightning are due to static induction effects ; their duration may be assumed to equal that experienced with direct lightning strokes, that is, up to several tenths of a second. In the course of this period the lightning current will vary between zero and several hundred amperes. With very short durations the current may even rise to 100–200 kA, but generally amperages will lie considerably below these maximum values. Current surges of 40kA are rare, while surges of 10–20 kA are a rather frequent concurrence. With regard to the polarity of thunder-clouds, the following data have been published in literature on the subject :

Country	Number of Measurements made	Polarity, % —	Polarity, % +	Author of reference.
Switzerland	12	86	14	Berger (1)
U.S.A.	734	93	7	Lewis & Foust (2)
Germany	1200	85	15	Grünewald (3)
Japan	?	approx. 97	approx. 3	Rokkuka (4)

This table shows that most of the overvoltages caused by direct lightning are of negative polarity. On the other hand, it must be expected that in the case of indirect lightning voltage surges will be more frequently of positive polarity. This fact can be of importance in installations operating at low voltages.

It is well known that the spark-over voltages for insulators equal those of rod-type spark gaps of the same length of flash-over. The characteristics of rod spark gaps are shown in Fig. 1. Here the impulse voltages are based on the so-called 50 per cent of a 1×50 wave, i.e. with a wave front of one microsecond. It is also seen that the influence of polarity is greater with the rod-disc spark gap than with the rod spark gap. The time after which spark-over occurs depends on the shape of the impulse wave front, and flash-over times will therefore be shorter the more abrupt is the effective wave front. In Fig. 2 the flash-over voltage is

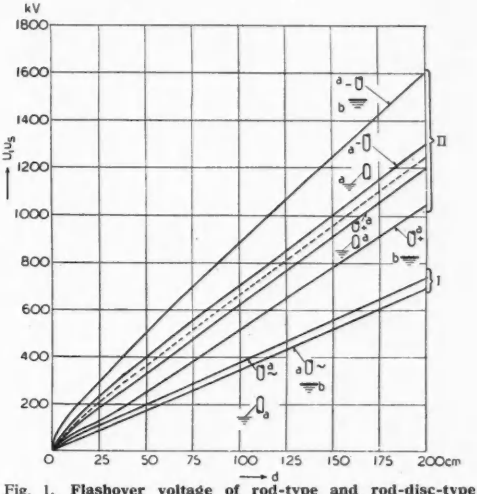

Fig. 1. **Flashover voltage of rod-type and rod-disc-type sparkgaps.**
I. For alternating current in kV eff.
II. For positive impulse voltage of 1/50 microsecond in kV max.
II. For negative impulse voltage of 1/50 microsecond in kV max.

charted as function of time-to-spark-over ; and it is seen that with decreased flash-over time (and increased steepness of the wave front) eventually a point is reached at which the influence of polarity ceases to

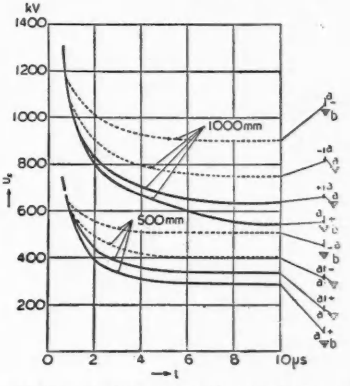

Fig. 2. **Flashover voltage versus time-to-flashover.**
Electrode positive relative to earth.
Electrode negative relative to earth.

prevail. This also applies to the flash-over of insulators, as can be seen from Fig. 3, where the flash-over ranges of a pin-type insulator with positive and negative polarity of the pin are compared to and co-ordinated with the characteristics of a rod-type spark gap. the latter being one metre in length.

In the case of transformer insulation (i.e. oil and paper) the break-down characteristic is of the kind shown in Fig. 4. Here the resistance of the insulation against breakdown remains constant over a certain time interval. The critical points *a* and *b* defining this interval are determined by the characteristics of the material. For high voltages *a* approximates to 2–3 microseconds, and *b* to 0.01–0.1 sec. With lower voltages *a* is found to range from 6 to 8 mircoseconds and *b* to one-hundredth to one-tenth second.

Rod-type spark gaps serve well as co-ordinated spark gaps for the protection of transformer insulation.

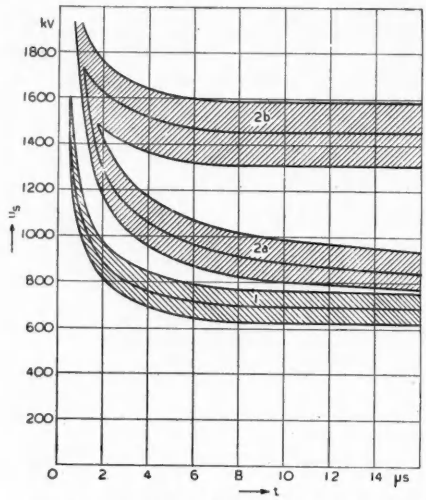

Fig 3. **Comparison and co-ordination of a pin-type insulator with rod-type and rod-disc-type sparkgaps designed to protect the insulator against both positive and negative voltage travelling waves.**

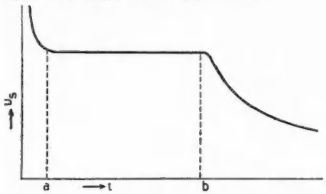

Fig. 4. **Insulation-level and break-down characteristic of transformer insulation as influenced by the time-element.**

This fact is illustrated by Fig. 5, where it is seen that the protective effect of the spark gap extends to very steep wave fronts as well as to less steep ones. The rod-gap which is independent of the polarity prevailing will reduce the flash-over voltage unnecessarily with less steep wave fronts; while this does not apply to negative overvoltages if a rod-disc gap is used. But ithe regard to positive overvoltages, the insulation level of the transformer will be reduced to a greater extent by the polarity-independent rod-type gap. Considering that negative overvoltages occur more frequently than positive ones, rod-disc type spark gaps afford a better utilisation of the insulation of high voltage transformers as well as of the insulators.

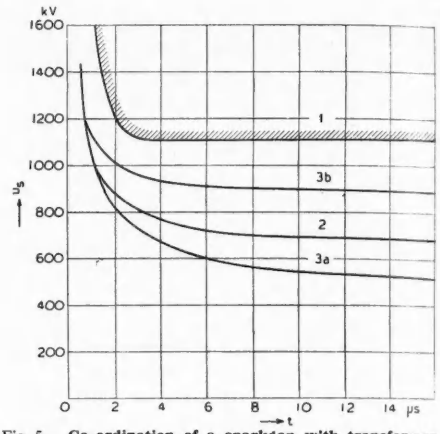

Fig. 5. **Co-ordination of a sparkgap with transformer insulation for protection of the latter.**
(1) Minimum insulation level of the transformer.
(2) Flash-over characteristcs of rod-type sparkgap of 1 m. length.
(3) Flash-over characteristics of rod-disc-type sparkgap of 1 m. length.

References.
(1) Bulletin S.E.V., 1936, p. 145.
(2) Electrical Engineering Trans., 1940, p. 227.
(3) C.I.G.R.E. 1939 Report, p. 323.
(4) C.I.G.R.E. 1939 Report, p. 321.

MODERN HARDNESS TESTING MACHINES

By DIPL.-ING. KURT MEYER. (From *Fertigungstechnik*, Vol. 1/77, No. 9, December, 1943, pp. 232-34).

WHERE the hardness testing of large quantities of identical or similar pieces is involved, rapidity of the test is important, without, however, sacrificing test accuracy. For this purpose, several types of testing machines have been developed to carry out hardness determination according to Brinell or Vickers. But no such mass-testing machines have been built in Germany for Rockwell tests.

While for other inspecting and testing purposes semi- or fully-automatic devices are available now, no such machines for hardness testing have yet been produced. But the development of such automatic hardness testing machines must be considered essential if hardness testing as such is to retain its position in mass production processes. It must, therefore, be considered fortunate that tendencies in this direction have become noticeable of late.

In the design of hardness testing devices for mass testing purposes, versatility of the instrument is definitely of secondary importance, more stress being laid upon rapidity of testing procedure and elimination of lost motion in handling the piece. Single purpose hardness testers can be generally divided into two groups, namely, external and internal testing devices, each group comprising two classes, which are (a) Determination of hardness according to Brinell or Vickers, and (b) Determination of hardness according to Rockwell.

MACHINES FOR EXTERNAL BRINELL AND VICKERS HARDNESS MEASUREMENTS.

Particularly for the application of normal and major load, a large range of well-tried single-purpose machines is available. With regard to the method employed in evaluating the depth of penetration achieved in the test, these machines can be grouped in two categories, i.e. (a) machines possessing an integral measuring device, and (b) machines without such device. Without doubt, the trend in the design of modern single purpose Brinell or Vickers hardness testing machines is towards the incorporation of the measuring device—mainly of the optical kind—in the machine itself, as this eliminates handling of the piece subsequent to the penetration test. For reasons of accuracy, mechanical measurement of the penetration can be employed only in machines where the measuring device forms an integral part of the machine so that measurement can take place during application of the test load.

Two different types of optical measuring device are in use, namely, microscopes coupled with a measuring device and projector devices with image screen on which a greatly magnified picture of the penetration is shown. Of these two optical types, the advantages lie with the projector type, since it is considerably less fatiguing to the eye, nor does it require any focal adjustment during operation of the machine.

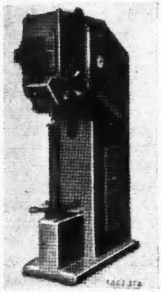

Fig. 1a.

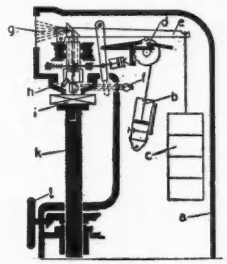

Fig. 1b.

At the present time instruments with projectors for the major load range are exclusively of the BRIVISKOP and of the DIA-TESTOR type. The image-screen instruments are built in standard as well as in numerous special designs. The major test load range is covered by the " BRIVISKOP 3000 " shown in Figs. 1a and 1b, which is built in two sizes. Its loading range extends from 62.5 to 3000 kg., with numerous intermediary loads, of which the majority correspond to standardised Brinell and Vickers loads. The loading pressure itself is generated by means of a tension spring. The desired speed of loading is obtained by turning the screw spindle of the needle valve of the dashpot. While complying with the condition that in standard procedure the full test load can be reached within 15 seconds in smooth operation, much shorter loading times, as short as 1-2 seconds, can also be obtained. These short loading times may, for instance, be used without hesitation in the mass testing pieces of heat treated or even hardened steels.

The image screen and the internal measuring device can be turned into various directions, thus facilitating evaluation of the penetration in different directions.

In actual test procedure, the control is set on its indicator dial at the desired loading pressure and the piece to be tested is then put on the test table. Thereupon the table is lifted into position until the test piece contacts with the head of the machine, the latter hereby clamping the piece down upon the table. This clamping action proves particularly useful when unwieldy pieces must be tested, holding them securely in place and preventing their shifting when the test load is applied.

As the image of the surface appears on the projector screen, it is easy to ascertain whether or not the spot selected for penetration is of suitable surface condition. By pressing the operating lever of the machine, the swivelling penetrator head (Fig. 1b) is turned into its vertical operating condition, that is, into the optical axis of the machine. Subsequently, the loading pressure is gradually built up until it has reached the predetermined magnitude. This is indicated by the load pointer

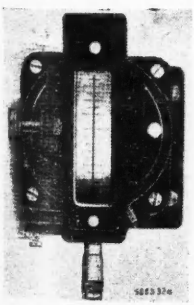

Fig. 2a.

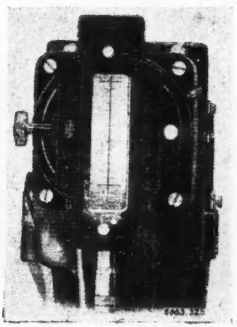

Fig. 2b.

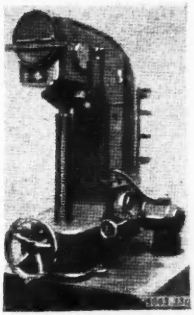

Fig. 3a.

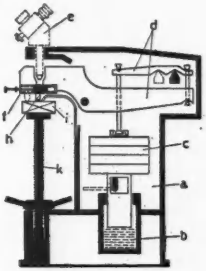

Fig. 3b.

moving over the dial of the instrument. The full test load is then held for the required length of time, and is then released by moving the aforementioned lever back into its inoperative position. This also moves the penetrator head back into its original position, so that the image of the penetration is now projected upon the screen. As shown in Figs. 2a and 2b, the image screen with its measuring device is of the turn-table type, which permits its positioning to any required angularity.

If the instrument is to be used for tolerance hardness testing, its frosted glass screen is replaced by another screen bearing the required tolerance marks. This method of using the hardness test is particularly suited to mass testing, since it is both rapid and foolproof and requires but little skill. In this way as many as 300 to 400 hardness tests can be carried out per hour.

Another instrument of this type is the DIA-TESTOR, Type 3a, shown in Figs. 3a, and 3b. This has a loading range of 120-3000 kg., allowing the adjustment to all standardised Brinell loadings from 187.5 to 3000 kg. as well as of the maximum Vickers standard load of 120 kg.

NOVEL Bending Device for Light Metal Tubing

(From *Fertigungstechnik*, No. 2, February, 1944, p. 33)

THIS device consists of a replaceable rotatable roll carried on a pillar, the roll radius equalling that of the bend to be produced. At the roll level a bending tool is provided which slides along a roller, being held in a forked guide. The bending tool is kept in place by the roll which projects into the fork. Both bending tool proper and guide are affixed to a lever pivoted on the rotatable upper part of the pillar. The proper position relative to the bending roll is obtained by adjusting a threaded spindle. At the end of the lever a locking device with handle is provided which permits rapid adjustment of the bending tool when inserting or withdrawing the tubing. The lower part of the pillar is furnished with a dial and an adjustable stop, which can be set to any bending angle desired. The device is arranged on a base plate which is easily bolted down to the work bench.

HIGH-PRESSURE LOCOMOTIVE, TYPE 232-P, WITH INDIVIDUAL AXLE DRIVE OF THE S.N.C.F.

By M. CHAN. (From *Revue Generale des Chemins de Fer*, Vol. 62, No. 5, Sept./Oct., 1943, pp. 101–109).

AN order for a 4,200 h.p. locomotive operating at 852 lb./sq. in. pressure with individual axle drives had been placed by the French National Railways in 1936. This locomotive was to be built jointly by the Société Alsacienne des Constructions Mécaniques, the firm of Schneider et Cie, and the Compagnie de Fives-Lille under certain licences granted to them by the Swiss firm Societé Winterthur. Although substantially completed in 1939 at the Graffenstaden shops of the Société Alsacienne des Constructions Mécaniques, lack of certain components due to war conditions delayed final assembly to such an extent that the first trial runs could not be made until early in 1943.

The salient features of this locomotive, which resembles the Hudson 232 type, can be seen in Figs. 1–4. As the photograph of the engine given in Fig. 1 was taken before completing encasement of the high pressure boiler, the fire tube portion of the latter can still be seen; while the three individual axle drives of the side shown can also be distinguished The high pressure boiler section includes the fire box and is of the water tube type, operating at 60 kg./cm.^{2}. A low pressure boiler of orthodox design is placed in front of the high pressure section, its operating pressure being 20 kg./cm.^{2}. The high pressure superheater, yielding a final steam temperature of about 400 deg. C., forms

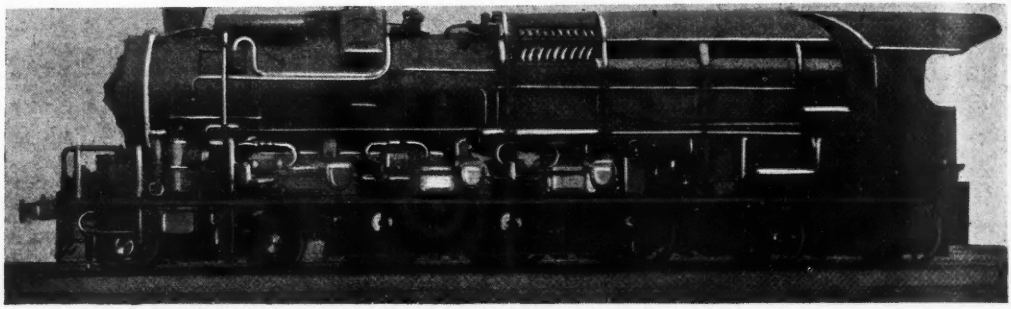

Fig. 1. **View of locomotive.**

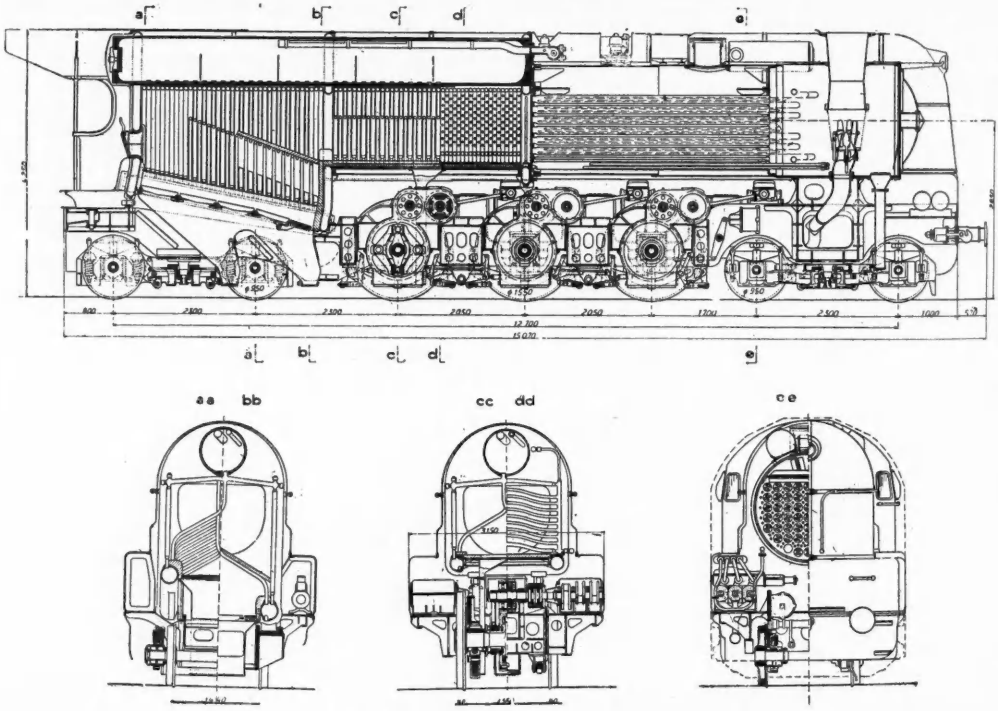

Fig. 2. **Sectional side view of locomotive.**

the final stage of the high pressure section, being interposed between the high pressure combustion portion and the low pressure boiler. The latter actually serves for preheating the boiler feed to 215 deg. C. and for supplying steam at 20 kg./cm.^{2} to the auxiliaries. As shown in Fig. 3b, a return bend type high pressure economiser (3) is inserted into the flues of the low pressure boiler from the flue gas inlet end of the latter. The superheater (5), passed by the 20 kg./cm.^{2} steam, consists of a number of return-bend type coils placed in certain of the lower flues. From the flues of the low pressure boiler the gases are finally discharged into the chimney equipped with the usual blast pipe (9).

Referring further to Fig. 3, the feed water is fed into the low pressure boiler by means of an ordinary injector, while it is withdrawn by a pump (6), Fig. 3, which passes it into the economiser (3) where its temperature is further increased, and finally into the high pressure boiler (1).

The high pressure boiler built for a working pressure of 60 kg./cm.^{2} consists of a seamless forged upper drum of 700 mm. dia. made of chromium-molybdenum steel. The bottom headers are connected with the drum by three boxheaders acting as downcomers, and by the riser tubes forming the walls of the fire box and combustion space. There is a fire-hole of usual dimensions in the front box header. The general arrangement of the evaporating tubes is shown in Fig. 5. Vertical and slightly curved tubes of 60 mm. inside and 70 mm. outside dia. compose the water walls, while inclined tubes of 62 mm. inside and 70 mm. outside dia. form the crown. All tubes are both expanded and welded. The spaces between the vertical riser tubes are filled with plastic refractory in order to prevent the leakage of air into the fire box. A casing of heat insulating material is kept in place by perforated sheeting.

The vacant space shown in Fig. 5 serves for the accommodation of the high-pressure superheater of special design. It is composed of a number of elements in grid form arranged in vertical planes. Fig. 6 shows one such superheater element, the tubing proper of 33 mm. inside and 40 mm. outside dia. extends between an upper saturated and lower superheated header, with the topmost superheater tube made of 52 mm. inside and 60 mm. outside dia. tubing. There is one saturated and one superheated header along each side of the boiler, each side serving to superheat the steam supplied to the three engines

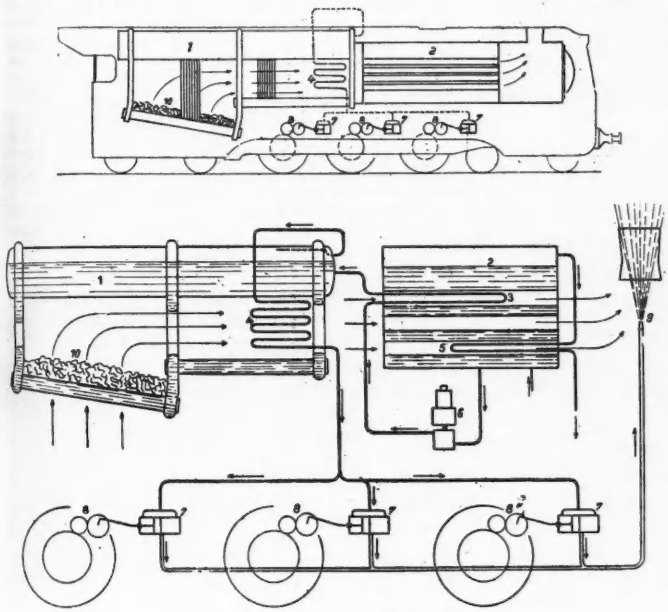

Fig. 3. **Steam circuit of locomotive.**

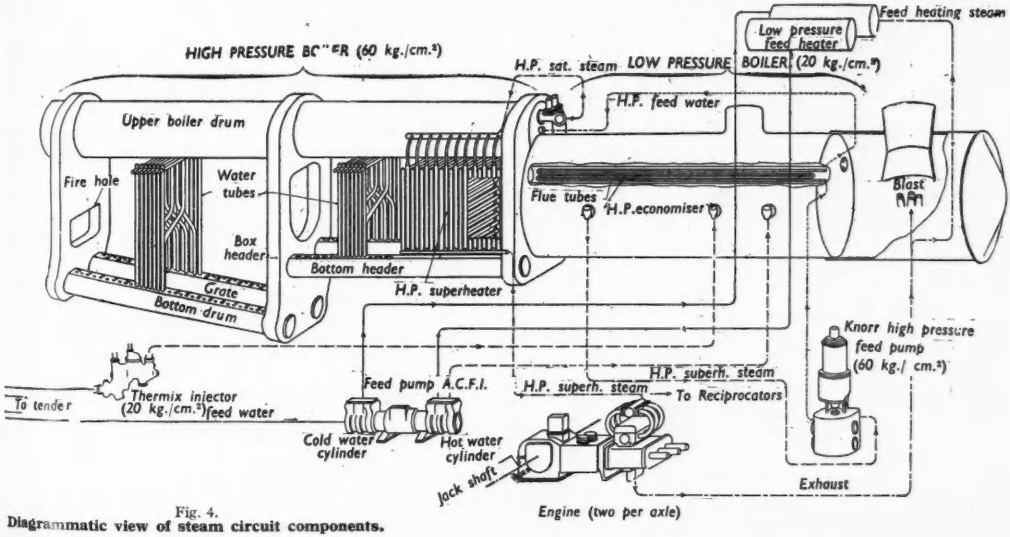

Fig. 4.
Diagrammatic view of steam circuit components.

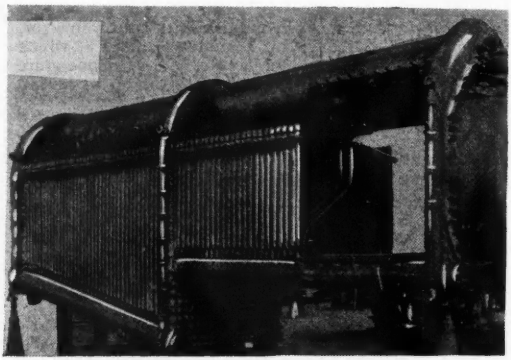

Fig. 5. **View of boiler (before final assembly).**

arranged on that particular side of the locomotive.

The low pressure boiler is of the ordinary locomotive type of a plate thickness of 18 mm. Its internal diameter is 1,718 mm. and its length is 3,800 mm. There are 57 flue tubes of 125 mm. inside and 133 mm. outside dia. and 77 small tubes of 33.5 mm. inside and 38 mm. outside dia., the flue tubes being used for the accommodation of the superheater and the economiser. The latter is composed of elements made of tubing of 32 mm. inside and 38 mm. outside dia. Only three flue tubes are occupied by the elements of the low pressure superheater, which superheater is composed also of tubing of 32 mm. and 38 mm. outside diameter.

The main purpose of the low pressure boiler, besides preheating the high-pressure boiler feed, is to free the latter from scale-forming matter and thus to prevent scale formation in the high-pressure boiler. Together, high-pressure and low-pressure boilers constitute one single assembly with seven-point support, of which six are movable, while the seventh is a fixed one, being the smoke box saddle support.

The feed water supply to the high-pressure boiler is effected by two Knorr feed pumps of special design, which are of the two-cylinder tandem type. Special float type equalising chambers are provided in order to prevent water-hammer. To maintain the respective outputs of the high-pressure and low-pressure boiler presents a special problem. In order to safeguard a sufficient water supply to the high-pressure boiler and also sufficient steam to the auxiliaries, a by-pass control is installed, by which high pressure steam can be injected into the low-pressure boiler while a reducing valve is installed to utilise high pressure steam for the operation of the auxiliaries, if required.

Each of the three driving axles is driven by two engines, having their corresponding cranks set at an angle of 180 degrees. A view of the engine unit is given in Fig. 7, while a longitudinal section is shown in Fig. 8. Each engine has three horizontal cylinders of

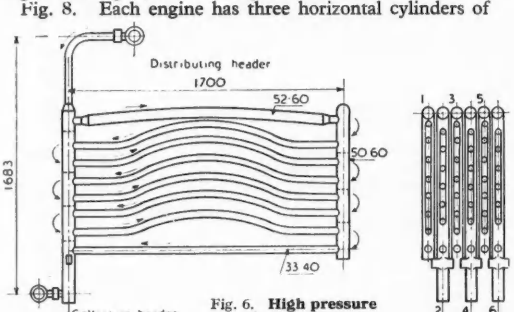

Fig. 6. **High pressure superheater elements.**

150 mm. bore and 255 mm. stroke operating on one crank shaft, the cranks of which are mutually placed at 120 degrees. As will be seen from Fig. 8, the engines operate on the simple expansion uniflow principle their speed being 1,000 r.p.m. at 148 km. per hour, and 800 r.p.m. at 120 km. per hour. The poppet valves are of the rotary cam type, each cam shaft being fitted with eight step cams. Six of these cover the fore gear range, the respective cut-offs being 10.0, 13.2, 15.9, 19.0, 25.0 and 70 per cent. The seventh cam provides a cut-off of 70 per cent in back gear, and the eighth cam constitutes mid-gear. In order to ensure that all six engines operate in the same gear, the respective cams are simultaneously operated by means of pressure-oil energised servo-motors, the latter being jointly actuated by the lever control. An electrically illuminated cam shaft position indicator is provided. The engines of each axle are coupled to a jack shaft by means of an elastic coupling of the Forst type, while a Winterthur transmission is placed between the jack shaft and the driving axle (Fig. 9). No special anti-slipping device is provided, but in the first fore-gear a very small valve lift is employed safeguarding equal steam distribution to the six engines.

The cylinder lubrication is of the usual type and presents no features of special interest. The two-gear

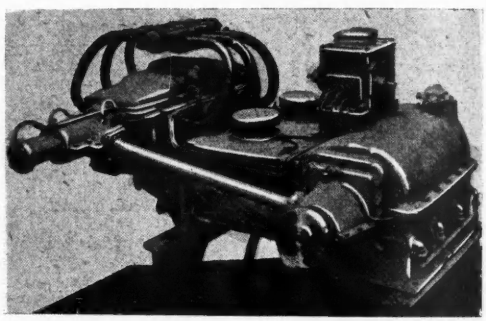

Fig. 7. **View of one of six reciprocators.**

type pressure oil pumps for remote control are chain driven from the foremost driving axle, and supply a high pressure lubrication oil system under 4–5 kg./sq. cm. pressure for operation of the servo-motors as well as a low pressure lubricating oil circuit at 1–2 kg./sq. cm. pressure. As these pumps are inoperative during standstill of the locomotive, a steam driven turbo-pump is also provided, the latter cutting out automatically when the locomotive gets under way. This control derives its impulse from the pressure variations in the oil circuits. Individual oil pumps are provided for the gear drives of the axles.

Both superheater and economiser are equipped with soot blowers. Of the auxiliary equipment, an automatic steam cooling device for the high-pressure superheater is worthy of note, the low pressure cooling steam being taken from the blast pipe circuit.

As the high-pressure boiler comes up to pressure more quickly when firing up than the low-pressure boiler, it is necessary to open the aforementioned by-pass valve in order to accelerate the pressure rise in the low-pressure boiler. Normally, from 3–4 hours are required to get up full steam pressure, the actual time depending upon the initial feedwater temperature and upon the firing rate. The salient data of the locomotive are as follows :—

High-pressure boiler :

Grate area 3.5 sq. m.
Pressure 60 kg./sq. cm.

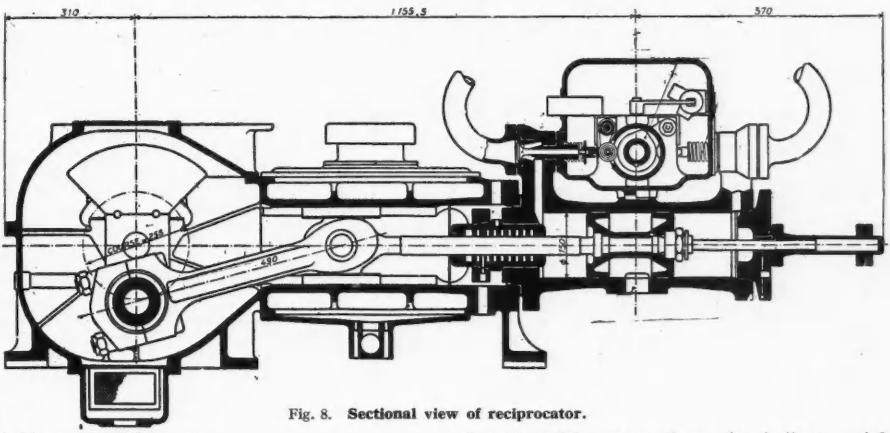

Fig. 8. **Sectional view of reciprocator.**

Cubic content 3.5 cu. m.
Boiler heating surface 44.0 sq. m.
Superheater heating surface 35.0 sq. m.
High pressure economiser surface (in low pressure boiler) 100.0 sq. m.

Low-pressure boiler :
Pressure 20 kg./sq. cm.
Cubic content 4.13 cu. m.
Boiler heating surface 125.8 sq. m.
Superheater surface 4.5 sq. m.

Engines :
Six engines of 3 cylinders each, bore 150 mm., stroke 255 mm.
Maximum output per engine, 700 h.p.
Driving wheel diameter 1.55 m.
Gear ratio 1.976.
Engine speed, 1,000 r.p.m. at 148 km. per hour.
Overall length of locomotive, including tender, 25 m.
Rigid wheel base, 4.1 m.
Total weight of locomotive, 126 tons.
Leading bogie weight, 30 tons.
Driving wheels adhesive weight, 64.8 tons.
Trailing bogie weight, 31.2 tons.

The employment of individual axle drives offers the advantage of permitting a reduction in wheel diameter and with it a reduction in the overall length of the locomotive, since in contrast with the orthodox locomotive design the wheel diameters need not be designed with any regard to piston speed. The elimination of coupling rods brought about by the employment of individual axle drives is not in itself a simplification of importance, as they are well adapted to high speed operation and are not a source of operational trouble. The main advantage of the individual axle drive is rather the facility with which it can be removed for repair and replaced by another unit. Thus repairs can be effected without having to take the locomotive out of commission. Only actual experience will be able to show whether or not the complication introduced by the employment of two boilers and by the individual axle drives will multiply the increased efficiency.

The expected fuel consumption figures of the locomotive per draw-bar h.p. are as follows :—

Locomotive Speed	1,500 kg.	1,750 kg.	2,000 kg.
80 km. per hour	0.825	0.845	0.880
100 " " "	0.920	0.920	0.930
120 " " "	1,150	1.090	1.080

At a speed of 100 km. per hour the locomotive develops approximately 2,300 draw-bar h.p. Actual test results are not available as yet, since the locomotive is only just being placed in service. But it can be stated that the trial runs made so far indicate satisfactory operation. In particular, starting has proved to be very easy.

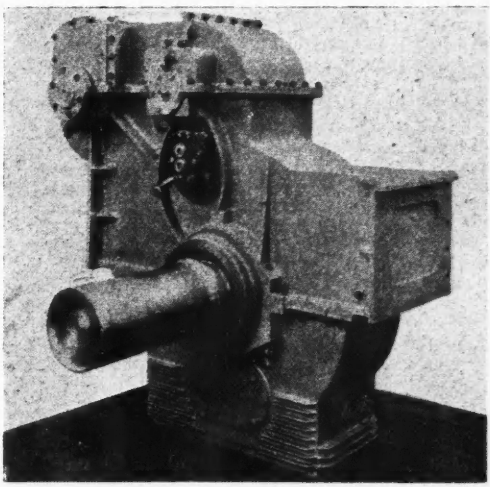

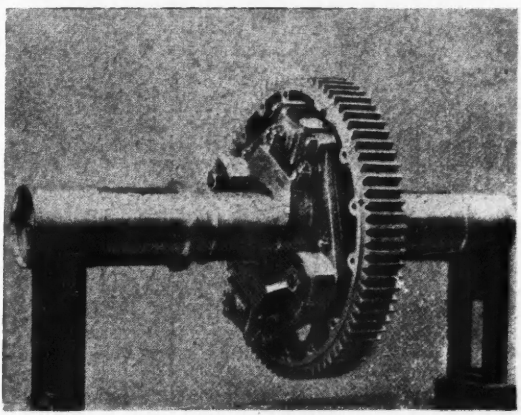

Fig. 9. **Geared axle drive.**

CLAMPING DEVICES FOR JIGS AND FIXTURES.

(From *Die Werkzeugmaschine*, Vol. 47, No. 6, March, 1943, pp. 129-132).

CLAMPING devices are used on jigs and machine-tools to fix movable components, such as slides, work supports compound slides, in the desired position. In indexing fixtures, particularly those of large size and where considerable thrusts must be absorbed, clamping devices are used to take off the index pin.

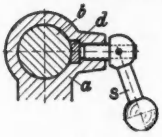

Fig. 1

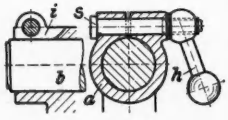

Fig. 2

A few typical clamping devices of this kind, which have proven satisfactory in practice, are shown in Figs. 1 and 2. Referring to Fig. 1, the pin *b* is fixed in position by the thrust exerted by the light alloy pad *d* by means of the screw provided with the clamping lever *s*. In Fig. 2, pin *b* is held in place by compressing the slotted holder *a* by means of bolt *s*, the nut of which is equipped with clamping lever *h*. By tightening the clamping lever *h*, shown in Fig. 3, fixing of the cylindrical piece *b* is accomplished through the pressure exerted by the clamping nut upon pad *d*.

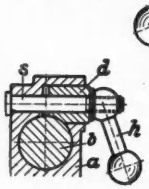

Fig. 3

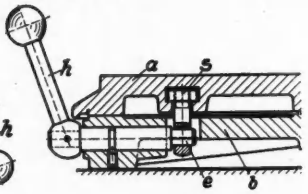

Fig. 4

Clamping of the rotary table *a* indicated in Fig. 4 is accomplished with the use of an eccentric-operated clamp, the eye bolt employed for clamping being fitted over the eccentric *e* of the bar carrying the clamping lever. Lengthwise movement of this bar is prevented by a dowel pin fitting into a recess of the bar.

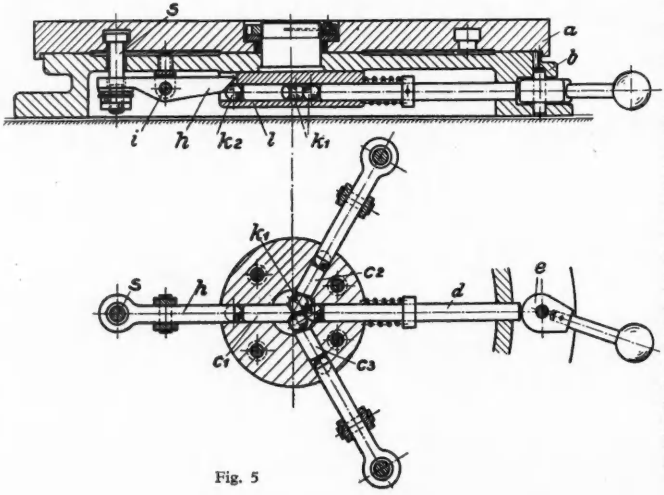

Fig. 5

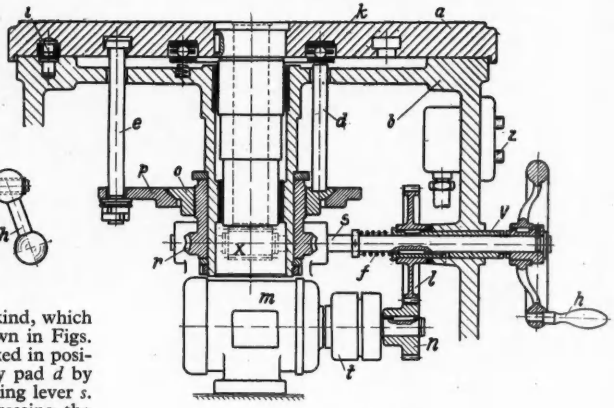

Fig. 6

A well-tried device for the synchronised multiple clamping of rotary tables is illustrated in Fig. 5. Here the thrust rod *d* actuated by the cam *e* of the clamping lever, transmits the pressure of the cam to three spherical steel balls k_1 which in turn transmit the cam thrust to the three thrust pins c_1, c_2 and c_3. The outer faces of these press upon the wedge-shaped faces of the three levers *h*, which pull down the three adjustable clamping bolts *s*. In order to safeguard even loading of the three thrust pins, c_1, c_2 and c_3, their faces abutting with the three steel balls, k_1, are appropriately slanted off, as will be seen in the lower part of Fig. 5.

An electrically operated fixing device applied to the rotary tables of large jigs and of machine-tools is shown in Fig. 6. Here fixing and release of the table *a* is effected by either pulling down or lifting the table. The lower push button of switch *2* is pressed if the table is to be fixed. This puts into operation the electric motor *m* which, through a friction coupling *t* and reduction gear *n* and *l* drives the worm gear drive *x* and *r*. Worm gear *r* forms part of a bush which rotates on the central sleeve of the stationary housing *b* which serves as bed for the rotary table. Above the worm gear *r* the bush has a threaded portion which serves as a lift screw for the travelling nut *o*. When travelling downward the latter pulls down annular flange *p* carrying the three clamping bolts *e*, which are arranged at 120 deg. from each other, and this downward movement is continued until table *a* rests securely on its bed. Vice versa, by pressing the upper push button of the switch, the motor and its drive revolve in the opposite direction and cause lifting of the table by means of the three lifting pins *d* attached to flange of the travelling nut *o*. A thrust bearing *k* is seen to be centrally arranged on the underside of the rotary table, this bearing taking the thrust exerted by the three lifting pins *d* and permitting easy rotation of the table for indexing. For the latter purpose a locating pin *l* is provided, which fits into the indexing holes on the under-

side of the rotary table. Rotation of the table for indexing is carried out by pushing in the hand-wheel *h*, until the gear wheels *l* and *n* are disengaged and then turning the hand wheel *h* in the required direction until the rotary table has reached its new position. The electric drive is so arranged that lifting or lowering of the table takes place only as long as the respective push button is pressed, the extreme positions of the table being indicated by the clicking sound caused by the slipping of coupling *t*.

A similar device operated by compressed air is shown in Fig. 7. Here the mechanism is actuated by a hand operated control valve *v* which energises the power cylinder *z*. The piston rod of the latter carries flange *c* containing three stud-bolts *s* screwed into the flange *o*. The latter carries three lifting pins *d* thrusting upward upon the ball bearing *k* in table *a* during the lifting stroke, while clamping down of the table is effected by the clamping pins *e*, which are pulled downward during the down stroke of the power piston in cylinder *z*.

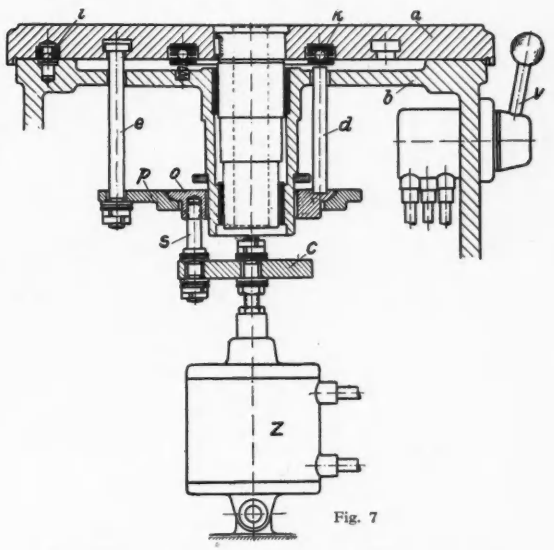

Fig. 7

SIMPLE INTERFEROMETER for SURFACE-QUALITY MEASUREMENT

By DIPL. ING. L. LEINERT. (From *Werkstattstechnik*, Der Betrieb, Vol. 37/22, No. 7, July, 1943, pp. 279-280).

IN present-day practice the production of highly finished surfaces should be based upon the attainment of definite minimum standards of surface quality and that means should be available for the reproduceable numerical measurement of surface condition. Such actual measurement when applied to a surface produced by a given mechanical process will constitute a ready means of deciding whether the specified surface quality cannot be produced equally well at lower cost by some other process. Thus, for instance, cases are known to the author where lapping could be abandoned in favour of the less expensive fine grinding without incurring a deterioration of the product. Several methods have been developed for the determination of surface roughness, the interference method being employed for the measurement of surface irregularities of less than 0.5 microns. In view of the regrettable fact that interferometric instruments have not so far been commercially available to any great extent, the following description of a simple instrument which has proved highly successful in industrial practice will be of interest.

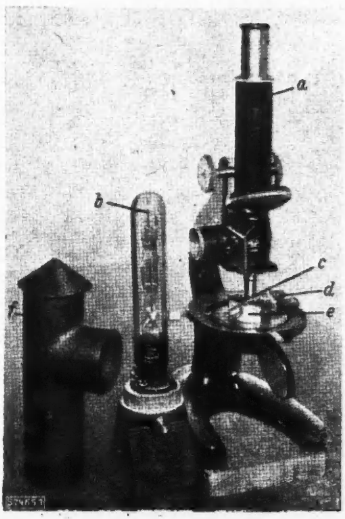

Fig. 1. **Interferometer.**
(a) Microscope with vertical illuminator
(b) Sodium lamp
(c) Transparent plane mirror
(d) Object to be examined
(e) Object holder
(f) Lamp housing

By the generation of Newton interference bands on reflecting surfaces, lines can be observed which represent the macrogeometric and microgeometric characteristics of the surface. These bands are produced by the mutual interference of two pencils of rays emitted by the same source of light, but travelling over different distances. If, at the point considered, this difference in the length of travel is an odd multiple of half a wave length, the light intensities will cancel each other out, thus causing darkness. Conversely, between these dark points, points of maximum light intensity will be produced by additive effect. These alternating dark and bright interference bands, if suitably magnified by optical means, make it possible to perceive existing irregularities of the surface inspected. This is due to the fact that these bands connect points of the surface which are equidistant from an optical datum plane, thus forming contours similar to those shown on topographic maps. As will be seen from Fig. 5 the magnitude of the serrations of the interference bands can serve as a measure of the degree of surface roughness. The magnitude of these serrations is measured in terms of the distance between successive interference bands, the latter distance always being equal to one-half wave length of the kind of light employed. The accuracy of surface roughness measurement will therefore depend upon the wave length emitted by the source of light. Thus, for instance, the use of sodium light permits the detection of surface irregularities as small as 0.05–0.6 microns.

While in the usual type of instrument the interference takes place within the microscope, thus requiring an optical system of very high quality, a new arrangement has been developed in which the interference originates externally to the microscope. The simplicity of set-up

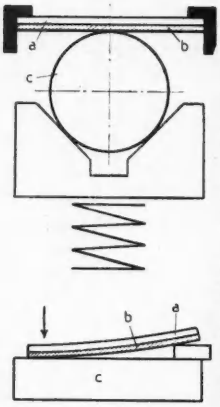

Fig. 2. **Arrangement of mirror plate.**
(a) Plane glass plate with silvering (b)
(c) Object to be examined

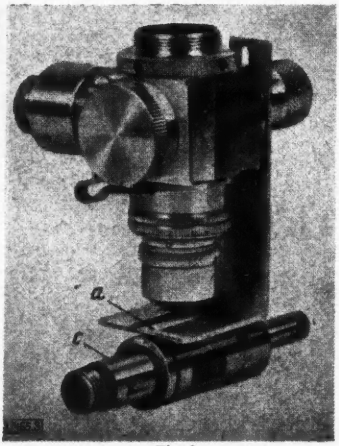

Fig. 3.
Attachment of mirror to microscope.

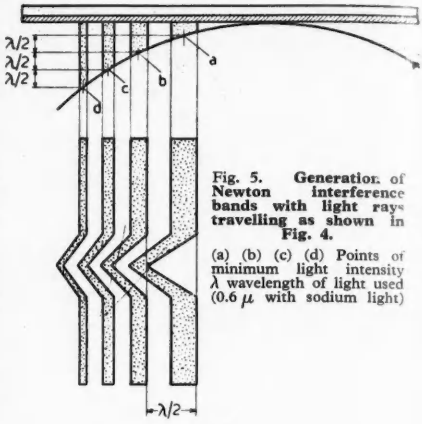

Fig. 5. **Generation of Newton interference bands with light rays travelling as shown in Fig. 4.**
(a) (b) (c) (d) Points of minimum light intensity
λ wavelength of light used (0.6 μ with sodium light)

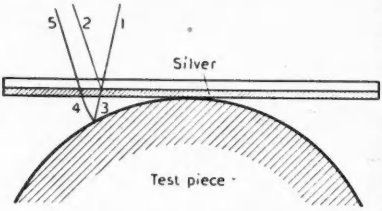

Fig. 4. **Travel of light ray with glass plate arranged as shown in Fig. 3.**

afforded by the new arrangement is evidenced by Fig. 1. Here the microscope *a* is an instrument of commercial quality equipped with a vertical illuminator. The source of light is a sodium lamp *b* emitting monochromatic light. Interference is produced by a partly transparent mirror which consists of a glass plate (Fig. 2) with the silver on its underside. This mirror is so placed that the silver touches the surface to be examined, as indicated in Figs. 2 and 3, the latter also showing the holder which keeps the mirror in place. Where plane surfaces are to be examined, the mirror is placed upon the surface in wedge-like fashion, as shown in Fig. 2. In this arrangement the desired interference bands are obtained by slightly pressing down the mirror. Mirrors of this kind may conveniently be made of cover glasses, the silver being a layer of aluminium applied by evaporation. Where the test piece has good reflecting powers, a silver with a reflecting power of 40 per cent will give best results. But even non-silvered cover glasses will yield weak interference bands which can be visually observed and photographed. Generally, a magnification of 150X is employed, the microscope being adjusted in the usual manner.

The working principle is outlined in Fig. 4, where a pencil of rays *1* is divided into a reflected pencil *2* and a pencil *3*, the latter penetrating the transparent silver and subsequently being reflected as pencil *4* by the surface of the piece. The reflected pencil *4* is passed through the mirror, from whence it emerges as pencil *5*. Owing to the fact that the length of travel of pencils *2* and *5* are different, mutual interference is produced, as illustrated in Fig. 5.

This instrument permits the investigation of surface irregularities ranging from 0.05–0.6 microns, provided that the surface possesses sufficient reflective power. Maximum and average surface roughness can be established by visual observation or from a photographic record, such as shown in Figs. 6-9. In addition to this, the regularity or irregularity of the tool marks observed can serve as a criterion of surface characteristic as such—at least within the small area examined. In determining surface roughness the interference bands should preferably be made to extend at right angles to the tool-marks, grooves, or scratches, which in high surface finish processing are usually unidirectional.

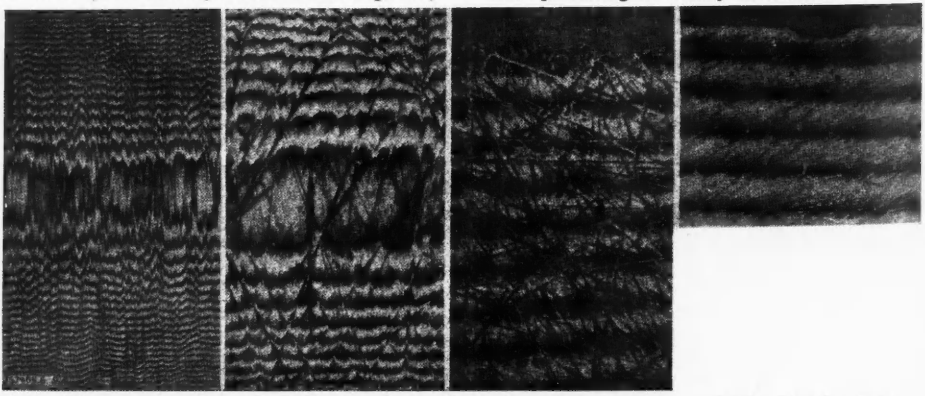

Fig. 6. **Precision ground surface.** Fig. 7. **Honed surface.** Fig. 8. **Lapped plane surface.** Fig. 9. **Honed surface.**

ANALYZING THE JET PROPULSION ENGINE

By COLIN CARMICHAEL. (From *Machine Design*, Vol. 16, No. 7, July, 1944, pp. 97-100).

SINCE the announcement some months ago that a twin-engined fighter plane employing jet propulsion had been successfully developed, no information has been released concerning engineering details. In an attempt to tie in the new development with established principles, the following discussion is offered.*

In the J.P. plane the jet is created by burning fuel in air, causing it to expand, with the result that it issues from a nozzle at high velocity.

Fig. 1 shows the principal features of a J.P. engine, which may be accommodated in a nacelle located in the wing. Air is drawn into the nacelle by a compressor, which delivers it at a pressure in excess of atmospheric into the combustion chamber. Here a series of fuel jets spray oil into the air where it burns, furnishing heat to raise the air temperature. Expansion of the heated air and combustion products furnishes the power to operate a turbine for driving the compressor and to produce the high-velocity jet for propulsion of the plane. More fuel may be burned beyond the turbine to provide additional jet energy.

Thrust and horsepower furnished by a jet are readily calculated. The well-known equation force equals mass times acceleration ($F = ma$), may be rewritten: force equals mass times rate of change of velocity ($F = mdv/dt$), or force equals rate of change of momentum. Assuming that the plane has forward velocity u feet per second while the speed of the jet (relative to the plane) is v feet per second, then the change of momentum of the air is $mv - mu = m(v - u)$. The rate of change of momentum is found by replacing m with the mass rate of flow of air in the jet, w/g, where w is the flow in pounds per second, giving the thrust equation

$$F = \frac{w}{g}(v - u) \quad .. \quad .. \quad (1)$$

The thrust horsepower is proportional to the thrust force times the velocity of the plane, or

$$thp = \frac{Fu}{550} = \frac{w(v-u)u}{550g} \quad .. \quad .. \quad (2)$$

Horsepower in the jet itself is proportional to the kinetic energy per second, or

$$jhp = \frac{w}{2g}\,\frac{v^2}{550} \quad .. \quad .. \quad .. \quad (3)$$

Ratio of thrust to jet horsepower is therefore

$$\frac{thp}{jhp} = \frac{2(v-u)u}{v^2} = 2\left(1 - \frac{u}{v}\right)\frac{u}{v} \quad .. \quad (4)$$

How this ratio varies with the ratio of plane speed to jet speed is shown in Fig. 2, from which it is evident that for a given jet (mass flow and velocity) the maximum thrust horsepower is developed when the plane speed is one-half the jet speed, that is, when the jet speed is twice the plane speed. The thrust, however, being directly proportional to the difference in speeds (eq. 1) is maximum when the plane is at rest, a fact which is of tremendous importance in take-off. The high thrust at low plane speeds is also effective in providing fast climb. As the plane speed approaches the jet speed, thrust falls off to nothing.

Propulsion efficiency may be found by comparing the thrust horsepower with the energy that must be added to the air to produce the jet. Inasmuch as the air enters the propeller or J.P. unit with velocity u relative to the plane, the energy to be added is $^1/_2mv^2 - {}^1/_2mu^2$ and the horsepower added is

$$php = \frac{w}{2g}\,\frac{v^2 - u^2}{550} \quad .. \quad .. \quad .. \quad (5)$$

which may be called the propeller horsepower. The efficiency is therefore

$$e = \frac{thp}{php} = \frac{2(v-u)u}{v^2 - u^2} = \frac{2\,\frac{u}{v}}{1 + \frac{u}{v}} \quad .. \quad (6)$$

Variation of efficiency with ratio of plane speed to jet speed is shown in Fig. 3.

In the jet-propulsion plane the mechanism which furnishes the jet is not subject to limitations due to attaining the speed of sound, and jet speeds may considerably exceed this value. Speed of the jet is a function of the ratio of fuel to air in the J.P. unit, a high percentage of fuel per pound of air resulting in high jet velocity but low propulsive efficiency unless the plane speed also is high.

To show the type of calculations that might be involved in designing for jet propulsion the following hypothetical figures are offered, assuming a plane speed of 525 miles per hour or 770 feet per second. A probable jet velocity may be calculated by considering what happens to the air which enters the nacelle at the forward end (Fig. 1). It will be assumed that the pressure in the combustion chamber is to be three times atmospheric. Part of this pressure increase may be acquired from the arrest of the incoming air but most of it is provided by a rotary compressor. At sea level the

*We thought it of interest to publish this article in spite of the fact that an identical jet propulsion engine is described in this issue by Prof. J. Ackeret. As to the usefulness of one or the other interpretation, the reader will have to draw his own conclusions.—*The Editor, E.D.*

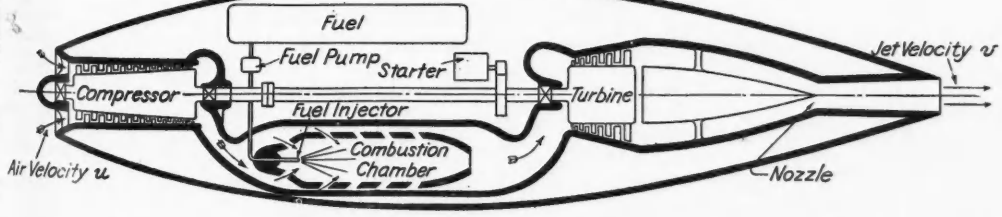

Fig. 1. Jet **propulsion engine consists primarily of a compressor, combustion chamber, gas turbine for driving the compressor, and a nozzle for producing the high-speed jet.**

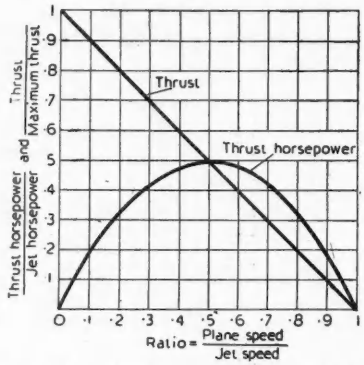

Fig. 2. **For a particular jet speed the thrust and thrust-horsepower are dependent on the plane speed.**

dynamic pressure would not exceed $\rho u^2/2 = .00237 \times 770^2/2 = 700$ pounds per sq. ft. = or 4.87 pounds per sq. in., ρ being the density of air at sea level, slugs per cubic foot. With compressor discharge pressure $3 \times 14.7 = 44.1$ pounds per sq. in., and intake pressure $14.7 + 4.87 = 19.57$, the pressure ratio is $44.1/19.47 = 2.26$. For this ratio and an air temperature of 50 deg. F, the horsepower is found to be 1.762 per pound of air per minute or 45.7 horsepower per pound of air per second. Assuming compressor efficiency 80 per cent, the horsepower absorbed will be $45.7/.8 = 57$, while the air will leave the compressor at a temperature of $50 + 133/.8 = 216$ deg. F.

With enough fuel burned in the combustion chamber to raise the temperature of the mixture, to say, 1500 deg. F., the total heat drop through the turbine and jet nozzle for the 3 to 1 pressure ratio will be 132 B.Th.U. per pound. Assuming turbine and jet efficiency 85 per cent, the available energy will be $132 \times .85 = 112.1$ B.Th.U. per pound per second or $112.1 \times 778/550 = 158$ h.p. Of this, 57 h.p. will be absorbed by the compressor, leaving 101 h.p. at the jet. From eq. 3 the jet velocity would therefore be $(2 \times 32.2 \times 550 \times 101)^{\frac{1}{2}} = 1900$ feet per second. Hence for a flow of one pound per second the thrust, given by eq. 1, would be $(1900 - 770)/32.2 = 35.1$ pounds and the thrust horsepower $35.1 \times 770/550 = 49$. Propeller horsepower (eq. 5) would be $(1900^2 - 770^2)/(2 \times 32.2 \times 550) = 85.2$, giving a propulsion efficiency of somewhat less than 60 per cent,

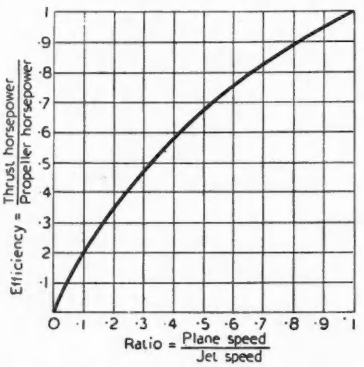

Fig. 3. **Propulsion efficiency of a jet is highest when the plane speed is only slightly less than the jet speed.**

compared with better than 80 per cent for a good modern propeller.

Translating the foregoing figures in terms of an actual plane, a fighter requiring, say, 2000 thrust horsepower at 525 miles per hour would use $2000/49 = 40.8$ pounds of air per second or 20.4 pounds per nacelle in a two-engine aircraft. The compressor plant would absorb no less than $40.8 \times 57 = 2330$ horsepower. This indicates the importance of the compressor and points to one of the reasons why the J.P. principle could not be applied many years ago. Hitherto rotary compressors have been of low efficiency and it is only since the development of a superior type of axial-flow compressor that both gas turbines and jet propulsion have become practically feasible.

Heat necessary to raise the air temperature from 216 deg. (at compressor discharge) to 1500 deg. (at turbine entrance) is approximately 0.26 (1500-216) = 334 B.Th.U. per pound, where 0.26 is the specific heat of air at constant pressure for this temperature range. Using an oil such as kerosine with heating value 18,500 B.Th.U. per pound, the fuel rate would be $334/18{,}500 = 0.018$ pounds per second. On the basis of propeller horsepower, this is a specific fuel consumption of $0.018 \times 3600/85.2 = 0.76$ pounds per h.p. hr., compared with less than 0.5 pounds per h.p.hr. for a modern petrol engine.

This high specific fuel consumption combined with low propulsion efficiency indicates that a jet-propelled plane working under the assumed conditions might be expected to use more than twice as much fuel as a conventional plane. This may be offset partly by the lighter weight of the J.P. engine, but shows that its use would be limited to short-range craft.

To improve the fuel consumption it would be necessary to increase the combustion temperature above the value of 1500 deg. F., used in the calculations. While available blade materials set a limit to the temperature that can be used in the turbine, higher temperatures can safely be used in the nozzle and jet. Consequently, a portion of the fuel can be burned in the main combustion chamber and the remainder in the passage beyond between the turbines and the nozzle. This adds to the energy in the jet and furnishes a higher jet speed which more than offsets the additional fuel that must be consumed. But for the same plane speed a higher jet speed means lower propulsive efficiency which partly offsets the gain in thermal efficiency. The conclusion is that only high-speed planes which can use a high-speed jet without unduly low propulsive efficiency can utilize jet propulsion effectively.

Advantages which justify its use in spite of high fuel consumption are, in addition to the higher speeds possible, the cheaper, less volatile fuel that can be used, the absence of vibration, and the difficulty of detection by the enemy due to the absence of propeller and exhaust noises as well as to the elimination of electrical ignition.

At high altitudes jet propulsion comes into its own. Although the jet plane, unlike the rocket, depends on atmospheric air and the power tends to fall off with decreasing density, it is much easier to provide the necessary air capacity to compensate for low density than it is in the case of a conventional engine. Hence high power is available at high altitudes while the resistance of the plane falls off, thus enabling the attainment of even higher plane speeds. Thermal efficiency also improves somewhat, consequently there is an all-round improvement in economy as well as in speed. Performance of the propeller plane, on the other hand, is limited by the fact that the propeller must work in atmospheric air, which at 30,000 feet has a density only 37 per cent of that at sea level. The J.P. unit has the advantage of being able to compress the air on which it works.

TECHNICAL NEWS

Announcements in this section include News relating to British Firms, and on Equipment produced by British Manufacturers.

Available literature may be secured by addressing a request to the advertising department of "The Engineers' Digest," or by writing direct to the manufacturer and mentioning "The Engineers' Digest" as a source.

- NEW EQUIPMENT
- BOOKS AND CATALOGUES
- BUSINESS CHANGES
- PERSONAL
- NOTES

PERSONAL.

Mr. Alex. D. Bailey, Vice-President of the Commonwealth Edison Co., Chicago, has been nominated President of the American Society of Mechanical Engineers.

Mr. G. Drury Baker, A.R.S.M., assistant chief engineer of the Consolidated Pneumatic Tool Co. Ltd., has been appointed Head of the Section of Fuel and Mining in the U.N.R.R.A.

Mr. J. D. Beddows, B.Sc., has been appointed metallurgist and technical assistant to Dr. E. G. West, of the Wrought Light Alloys Development Association.

Mr. Thomas Campbell Finlayson, M.Sc. (Manch.), M.I.Chem.E., has been appointed technical director to the Woodall-Duckham Vertical Retort and Oven Construction Co. (1920) Ltd.

Mr. D. P. Edkins has been appointed assistant chief designer to the Westland Aircraft Co. Ltd.

Mr. R. Laroux Handley has been appointed foundry manager to Ferranti Ltd., in succession of **Mr. Frank Andrew,** who retired from this position but will continue in the capacity of technical adviser and consultant on foundry matters to serve the company.

Mr. J. H. Hart, who is employed in the Electrical Measuring Instrument Department of Elliott Brothers (London) Ltd., has completed 60 years' service with the firm.

Mr. George Hey, M.I.Mech.E., has retired from the Hey Engineering Co. Ltd., Coventry. **Mr. S. B. Wright, M.I.P.E.,** has been appointed managing director, and **Mrs. O. M. Simpson** remains as director and secretary of the company.

Mr. C. S. LeClair, M.I.Mech.E., has been appointed technical director, and **Mr. E. G. Taylor,** sales director of Tecalemit Ltd.

Mr. E. F. Mitchell has been appointed regional manager of the Dunlop Rubber Co. Ltd., for the Midlands, with headquarters in Birmingham.

Sir Samuel Osborn, a former Lord Mayor of Sheffield, chairman of Samuel Osborn and Co. Ltd., celebrated recently his 80th birthday.

Mr. T. S. Parkinson, A.M.I.E.E., has been appointed deputy borough electrical engineer of the St. Helens Corporation Electric Supply.

Sir Harry Railing, chairman of The General Electric Co. Ltd., has been elected President of the Institution of Electrical Engineers.

Mr. E. W. Steele and **Mr. T. Fraser** have been elected to the board of Metropolitan Vickers Electrical Co. Ltd.

Mr. H. Taylor, A.M.I.P.E., has been appointed to the Pitter Gauge and Precision Tool Co. Ltd., as technical representative to cover Lancashire, Cheshire and part of the West Riding as far east as Bradford.

NEW EQUIPMENT.

INCREASING PRODUCTION WITH SYNTHETIC RESIN ADHESIVES.

SPOT GLUING WITH THE HIGH FREQUENCY HEATING GUN DEVELOPED BY MESSRS. PYE TELECOMMUNICATIONS LTD., CAMBRIDGE.

THIS high frequency gun makes it possible to apply heat locally to a synthetic glue so as to cause it to set rock hard within a short space of time. The area heated by the gun is circular with a diameter of about ½". The adhesive outside the heated spot is unaffected in properties, and if the correct type is used will eventually harden at shop temperature to produce a complete bond.

It is thus possible to build up an assembly in a jig by "spot gluing" and to remove it from the jig immediately. Overall setting of the adhesive then takes place whilst the assembly is awaiting further operations.

When building ribs and similar aircraft structures the plywood biscuits can be rapidly "spotted" in place with the gun and the use of brads avoided.

Similarly, plywood stiffening strips can be fixed to plywood skins. The strip is coated with adhesive and held in place on the skin in a simple jig. The gun is then applied for a few seconds (the time depending on the thickness of the plywood used) to spots at a pitch of 1-1½". The cured spots hold the strip firmly in place and eliminate the use of clamps or other pressing devices whilst the remainder of the glued area hardens normally.

The high frequency gun simplifies the operation of laying up tailored veneers on a shaped mould for the production of plywood of double curvature.

Considerable difficulty is experienced at present in the edge gluing of successive veneers together on the mould. The standard practice of heating the glue line with a soldering iron and applying side pressure by hand is slow and somewhat uncertain. Paper tape or metal staples can be used, but must be located in positions where they can be removed so that they do not remain in the finished article.

HEAT TREATMENT SPECIALISTS

ON APPROVED LIST OF AIR MINISTRY AND ADMIRALTY

- Case Hardening and straightening up to 8 ft. long.
- Hardening all Classes of Sub. and High Speed Steel Tools, Bakelite Moulds and Press Tools.
- Hardening by the Shorter Process.
- Cyanide Hardening, Capacity 3 tons per week
- Springs: Any size, shape or quantity.
- Aluminium Alloys Heat Treated to A.I.D. Specifications.
- Heat Treatment of Alloy Steels up to 10 ft long
- Heat Treatment of Meehanite Castings, etc.
- Crack detecting on production lines.
- Chemical Rustproofing (different colours) to A.I.D. and other Specifications.

THE EXPERT TOOL & CASE HARDENING CO. LTD.
(Est. 1918)
GARTH ROAD, LOWER MORDEN, SURREY.
Telephone: Derwent 3861-2

Bristol for Engineering—
BRISTOL FAMOUS FOR:—
Mechanical, Electrical, Constructional, Aeronautical and Marine Engineering.
Consult the BRISTOL ENGINEERING MANUFACTURERS' ASSOCIATION, 104, FILTON AVENUE, BRISTOL, 7

By means of the high frequency gun the veneers can be spot glued together with rapidity and security. The spots are widely spaced in places where the curvature is slight and are crowded together where curves are severe.

Synthetic resin glues such as Aerolite 304F are particularly suitable for this operation. Skin glue and formaldehyde can also be used.

The radio frequency power of about 100 watts at 170 megacycles is supplied by a self-oscillator which together with its power unit is housed in a steel case 10″ × 8″ × 18″. The oscillator weighs only 45 lbs. and is easily lifted therefore by the carrying handles provided. The high frequency power is applied to the work by means of a gun connected to the oscillator by a flexible concentric transmission line. Tuning is accomplished by sliding a button on the top of the gun which carries a lamp which is brightly lit by the high frequency current at the position of correct tuning.

The power is automatically switched on when the gun is pressed on to the work, and is then automatically switched off after a predetermined interval by a timing circuit in the transmitter unit. The time interval can be set at any value up to 12 seconds by a dial on the transmitter. The time required to cure the glue depends, of course, on the thickness of the veneer, but glue lines beneath 2 mm. veneers may be cured in 2 secs. The apparatus is designed to work off a 190-240V. 50 cycles supply and the input power required is 600 watts. Other electrode assemblies have been developed to enable the transmitter to be used in preheating plastics prior to moulding.

High frequency guns are available only for work of national importance and of high priority. All enquiries and requests for demonstrations should be made to the distributors, Messrs. Aero Research Limited, Duxford, Cambridge (Telephone: Sawston 167-8).

Rotary Louvre Plant. The latest publication of Messrs. Dunford and Elliott (Sheffield) Ltd., 54, Victoria Street, London, S.W.1., describes the construction and operation of the Rotary Louvre Plant. This plant has many applications such as drying, cooling, impregnating, roasting, cleansing of non-ferrous swarf, evaporation, and can also be used as a general reaction vessel.

For operation under special conditions, the portions of the mild steel drum which are in contact with the material under treatment can be coated with rubber, ebonite, copper, aluminium alloys, or with various proprietory coatings and enamels.

Copies of the illustrated brochure, which contains a list of about 100 different materials which can be processed by the Rotary Louvre Plant, can be obtained free on application.

The Rotary Louvre Plant is manufactured in U.S.A. and Canada under licence by the Link-Belt Company of Chicago.

BOOKS RECEIVED.

JARU Compensating Bearing. A leaflet published by The Joint Aeronautical Research Unit, Warren Row Factory, near Reading, presents an illustrated description of the Jaru compensating bearing. The bearing consists of an outer shell and a bronze liner split radially into a number of segments, each segment being bonded to the other and to the outer shell by a suitable grade of natural or synthetic rubber. The bearing can be used for supporting a sliding or rotating tubular member, and can adjust itself to accommodate bending deflections in the length of, and ovalling in the cross-section of the tube. It can be designed to meet individual requirements in a number of applications.

Ideal Factory Heating. The 16-page brochure just issued by Messrs. Tangyes Ltd., gives interesting details on the Tangye heating stove developed recently by the Cornwall works. New features of the stove are :—large radiation surface area ; maximum heat from fuel ; effective control of combustion ; and interchangeable sections. Write for free copy of the brochure to Tangyes Ltd., Cornwall Works, Smethwick, Birmingham.

Own Sales Organisation of Legg (Industries) Ltd. Legg (Industries) Ltd., Manufacturers of Electrical Equipment, Williamson Street, Wolverhampton, have decided to build up an own sales organisation which will handle, commencing September, the sale and distribution of the company's products.

REQUIRED FOR APPOINTMENT WITH PROSPECTS IN BIRMINGHAM

AN ENGINEER

Preferably with administrative experience, 30–35, with practical knowledge of the setting up and performance of machine tools as used in the light engineering industry and of the fixing of operation and machine times. Write Box No. 77, *The Engineers' Digest*, 120, Wigmore St., London, W.1.

SENIOR ENGINEERS, DESIGNERS and DRAUGHTSMEN required for Automobile Manufacturing Company in the Midlands. State experience, apprenticeship and salary expected. Box 0007, Advertisement Dept., *The Engineers' Digest*, 120, Wigmore St., London, W.1.

Legg

for

BATTERY CHARGING EQUIPMENT AND METAL RECTIFIERS

for all purposes

LEGG (Industries) LTD., WILLIAMSON ST., WOLVERHAMPTON

M-W.18

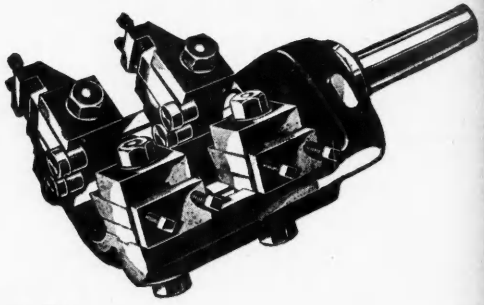

2 Diameters - ONE operation

This DOUBLE BOX TOOL is designed to form two diameters at one operation—one with the front set of cutters, and one with the back set . . . Maximum diameter 2¼ ins. up to a maximum length of 7 ins. . . . Also supplied with an Adaptor to suit the turret . . . Early delivery.

ACKWORTHIE

PRECISION MACHINE TOOLS

JOHN ACKWORTHIE LTD., BIRMINGHAM, 14

Telephone : WARSTOCK 2201/2/3.